Supporting Information for

Dynamic Solvent System as a novel approach to sustainable MOF crystallization

Leonid Shupletsov[a], Alina C. Schieck[a], Irena Senkovska[a], Volodymyr Bon[a], Stefan Kaskel[a, *]

[a] Chair of Inorganic Chemistry I, Technische Universität Dresden, Bergstraße 66, 01069 Dresden, Germany, *e-mail: stefan.kaskel@tu-dresden.de

Content

Methods

Synthesis of $NiBDP_{Lit.}$ (Reflux synthesis)

The synthesis was adapted from the literature. [1] In a degassed Schlenk tube, H_2bdp (100 mg, 475 µmol, 1 eq.) was suspended in 10 ml of degassed DMF. The suspension was stirred at 60 °C for 1 h. Then, under an argon counter flow, $Ni(NO_3)_2 \cdot 6H_2O$ (138 mg, 475 µmol, 1 eq.) was added to the mixture, which subsequently was heated to reflux and stirred for 5 more hours. After cooling to rt the orange precipitate was collected via centrifugation and washed with DMF (3x10 ml) to obtain 111 mg of product after desolvation. (Yield: 87 %).

General procedure for the synthesis of NiBDP (Solvothermal synthesis)

To a 50 ml Schott flask, H_2bdp (53.5 mg, 255 µmol, 1 eq.) was added together with the corresponding solvent, or solvent mixture (see Table S1). The mixture was sonicated briefly (5 min) to generate a white suspension. To the suspension, $Ni(NO_3)_2 \cdot 6H_2O$ (74.0 mg, 255 µmol, 1 eq.) was added. The mixture was sonicated again until all of the metal salt dissolved (5 min), and a pale green suspension was obtained. The flask was placed in a preheated oven at 150 °C for 24 h, unless stated otherwise. After cooling to rt the obtained orange solid was collected via centrifugation and washed with NMP (3x10 ml) and DMF (2x10 ml), unless stated otherwise. The crystals were kept in DMF for at least 3 h, removed from the mother liquor by filtration, and dried in air. Yields typically ranged between 60 and 90 % depending on the specific procedure.

Screenings were conducted at 1/5th of the given amounts in 10 mL scintillation vials. A scale-up of the **$NiBDP_{B+AA}$** 3.50 M synthesis was performed by employing fivefold reagent quantities in a 250 ml Schott flask.

Table S1. Volumes of the utilized DSS components for all solvothermally synthesized [**Ni(bdp)]$_n$** samples.

Material	V_{BuOH} / ml	V_{DMF} / ml	V_{AA} / ml	≈c_{AA} / mol/L
$NiBDP_D$	0	15	0	0
$NiBDP_{D+AA}$	0	15	1.25	1.35
$NiBDP_B$	15	0	0	0
$NiBDP_{B+AA}$ 0.55 M	15	0	0.50	0.55
$NiBDP_{B+AA}$ 1.35 M	15	0	1.25	1.35
$NiBDP_{B+AA}$ 2.50 M	15	0	2.50	2.50
$NiBDP_{B+AA}$ 3.50 M	15	0	3.75	3.50
$NiBDP_{B+AA}$ 4.35 M	15	0	5.00	4.35
$NiBDP_{D+B+AA}$	15	15	2.50	1.35

Synthesis procedure of $NiBDP_{B+AA*}$ (Solvothermal synthesis)

In a 50 ml Schott flask, BuOH (15 ml) and AA (3.75 ml; ≙ 3.50 M) were mixed and sealed. The flask was heated to 150 °C for 72 h and cooled to rt. To the reacted solvents, H_2bdp (53.5 mg, 255 µmol, 1 eq.) and $Ni(NO_3)_2 \cdot 6H_2O$ (74.0 mg, 255 µmol, 1 eq.) were added and sonicated until the metal salt completely dissolved (10 min). The flask was sealed again and heated to 150 °C for 24 h. After cooling to rt the obtained orange solid was collected via centrifugation and washed with NMP (3 x 10 ml) and DMF (2 x 10 ml). The crystals were kept in DMF for at least 3 h, removed from the mother liquor by filtration, and dried in air to yield 44.7 mg (72 %) of orange crystalline powder after desolvation.

General procedure for the synthesis of [Zn(bdp)]$_n$ (Solvothermal synthesis)

To a 50 ml Schott flask, H_2bdp (53.5 mg, 255 µmol, 1 eq.) was added together with the corresponding solvent or solvent mixture (See Table S2). The mixture was sonicated briefly to generate a white suspension. To the suspension, $Zn(NO_3)_2 \cdot 6H_2O$ (76.5 mg, 255 µmol, 1 eq.) was added. The mixture was sonicated again until all of the metal salt dissolved. The flask was placed in a preheated oven at 150 °C for 24 h. After cooling to rt the obtained colorless solid was collected via centrifugation and washed with NMP (3 x 10 ml) and DMF (2 x 10 ml), unless stated otherwise. The crystals were kept in DMF for at least 3 h, removed from the mother liquor by filtration, and dried in air. Yields typically ranged between 70 and 90% depending on the specific procedure.

Screenings were conducted at 1/5th of the given amounts in 10 ml scintillation vials.

Table S2. Volumes of the utilized DSS components for all solvothermally synthesized [**Zn(bdp)]$_n$** samples.

Material	V_{BuOH} / ml	V_{DMF} / ml	V_{AA} / ml	≈c_{AA} / mol/L
ZnBDP$_D$	0	15	0	0
ZnBDP$_{D+AA}$	0	15	1.25	1.35
ZnBDP$_B$	15	0	0	0
ZnBDP$_{B+AA}$ 0.30 M	15	0	0.25	0.30
ZnBDP$_{B+AA}$ 0.55 M	15	0	0.50	0.55
ZnBDP$_{B+AA}$ 1.35 M	15	0	1.25	1.35
ZnBDP$_{B+AA}$ 3.50 M	15	0	3.75	3.50
ZnBDP$_{D+B+AA}$	15	15	2.50	1.35

Sustainable washing method 1.

Instead of NMP and DMF, the samples were washed with DMSO (3 x 10 ml) and EtOH (3 x 10 ml) prior to activation. The samples washed with this method are denoted as “DMSO/EtOH”.

Sustainable washing method 2.

The product was removed from the mother liquor and placed into a 30 ml Soxhlet thimble. The thimble was inserted into a Soxhlet apparatus, and the extraction was performed with pure butanol overnight. 200 ml of butanol were loaded into the apparatus, which could be reused for at least 8 samples. The samples washed with this method are denoted as “Soxhlet”.

TGA/DTA

Thermal analysis was performed on a NETZSCH STA 409C/CD in a synthetic air (80/20 nitrogen/oxygen) atmosphere at 5 K min^{-1} heating rate. Samples were analysed before or after desolvation. In all cases, the residual mass of the sample at T = 250 °C was considered as the mass of the desolvated MOF.

NMR

^{1}H Nuclear Magnetic Resonance (NMR) spectra were acquired using a Bruker Avance III HD 300 MHz spectrometer using DMSO-d_6 as the solvent and benzene or dibromomethane as an internal standard at 25 °C. The chemical shifts were calibrated using the residual proton signal or the solvent. NMR of digested MOF samples was conducted by dissolving 7-10 mg of the MOFs in 0.1 ml of 37 % DCl in D_2O,

and then solubilizing the resulting suspension in 0.5 ml DMSO-d6 with dibromomethane as internal standard.

ICP OES and residual mass analysis

ICP OES analysis of the solvent after MOF synthesis was conducted with an ICP OES Optima 7000 DV from Perkin Elmer equipped with the autosampler S10. For that, 5 ml of the mother liquor was filtered to remove solid residues of the MOF particles, and the liquid was fully removed by drying at 180°C overnight. The solid residue was weighed and dissolved in 1 ml of HNO_3 (65 %). The obtained solution was then diluted to 50 ml with ultrapure water. The contents of Zn and Ni were then determined at emission wavelengths of 206.200 nm and 231.604 nm, respectively. Three scans were made per sample, and the average value is reported.

Nitrogen Physisorption

Nitrogen adsorption isotherms were obtained at 77 K with a Belsorp Max II instrument. Prior to the measurement, approx. 20 - 30 mg of the MOF sample was activated from the respective solvent at 150 °C under dynamic vacuum for at least 4 h, but usually overnight. The determined pore volume was compared to the theoretically calculated value from crystal structures of the solvated state. The calculations were performed with Mercury software,[2] and Poreblazer.[3]

Conductometric Titration

Conductometric titration was performed with two stainless steel electrodes at d = 1 cm. The VMP-3 potentiostat from Biologic, controlled with the EC-Lab software V11.27 was used for conductivity measurement.

SEM

SEM images were taken with secondary electrons in a HITACHI SU8020 microscope using 2.0 kV acceleration voltage and 8 mm working distance. The sample powders were prepared on a sticky carbon sample holder and sputtered with gold before the measurement.

VLM

Visual light microscopy images were acquired with the Olympus GX53 microscope equipped with the Olympus DP74 camera. The size measurement was performed with the Olympus Stream Essentials software package.

PXRD

Powder X-ray diffraction (PXRD) patterns were collected in transmission geometry on a STOE STADI P diffractometer operated at 40 kV and 30 mA with monochromated Cu-$K_{\alpha1}$ (λ = 0.15405 nm) radiation with a scan speed of 180 s/step and a step size of 6°.

Pawley refinement

Pawley refinement of selected PXRD patterns was conducted using Reflex module of Materials Studio 5.0 software. The Pseudo-Voigt profile function and Berar-Baldinozzi asymmetry function were used for profile fit.[4]

Single-crystal X-ray diffraction

A single crystal of $[Ni(bdp)]_n$ was prepared in a borosilicate glass capillary (d = 0.3 mm) with a small amount of solvent. The data set was collected at the BL14.2 beamline of the BESSY II synchrotron, operated by Helmholtz-Zentrum Berlin für Materialien und Energie.[5] Four images from different crystal

orientations were collected in order to determine the crystal symmetry and scan angle range using the iMosflm program.[6] The φ scan with an oscillation step of $\Delta\varphi$ = 0.1° was used for the collection of 1800 frames, which were processed automatically using XDSAPP 2.0 software.[7] The crystal structures were solved by direct methods and refined by full-matrix least-squares on F^2 using the SHELX-2018/3 program package.[8] All non-hydrogen atoms were refined in an anisotropic approximation. Hydrogen atoms were refined in geometrically calculated positions using a riding model with U_{iso}(H) = 1.2U_{iso}(C).

Single crystals of $[Zn(bdp)]_n$ (**ZnBDP$_{D+AA}$**) and BUT-58 (**ZnBDP$_{B+AA}$** 3.50 M AA) were prepared in a nylon loop using perfluorinated PARATONE® oil. The data sets were collected on an XtaLAB Synergy diffractometer (Rigaku Oxford Diffraction), equipped with a 4-circle goniometer, Mo-microfocus tube, and Eiger 2R 1M CdTe detector (DECTRIS). Molybdenum K$\alpha_{1,2}$ radiation (λ = 0.71073 Å) was used for the data collection, conducted at 298 K. CrysAlisPro software (V.42.95a) was used for the data collection and processing.[9] The ω- and φ- scans with an oscillation step of $\Delta\varphi$ = 0.3° were used for the collection. The diffraction images were processed automatically in CrysAlisPro, and semi-empirical multiscan absorption correction was applied. The crystal structures were solved by direct methods and refined by full-matrix least squares on F^2 using the SHELX-2018/3 program package.[8] All non-hydrogen atoms were refined in an anisotropic approximation. Hydrogen atoms were refined in geometrically calculated positions using a riding model with U_{iso}(H) = 1.5U_{iso}(C) for CH_3 and U_{iso}(H) = 1.2U_{iso}(C) for all other carbon atoms.

CCDC 2426284-2426286 contains the supplementary crystallographic data for $[Ni(bdp)]_n$, $[Zn(bdp)]_n$, and BUT-58, respectively. These data can be obtained free of charge from the Cambridge Crystallographic Data Centre *via* www.ccdc.cam.ac.uk/data_request/cif.

Table S3. Crystallographic parameters of $[Ni(bdp)]_n$, $[Zn(bdp)]_n$, and BUT-58.

	$[Ni(bdp)]_n$	**$[Zn(bdp)]_n$**	**BUT-58**
Appearance	Orange needle	Colorless block	Colorless block
Empirical formula	$C_{14}H_8N_4NiO_2$	$C_{12}H_8N_4O_{11.2}Zn$	$C_{12}H_8N_4Zn$
Formula weight	322.93	452.79	281.62
Crystal system	orthorhombic	tetragonal	tetragonal
Space group	*Imma*	$P4_2/mmc$	$I4_122$
a (Å)	22.000(4)	13.2864(2)	16.3434(2)
b (Å)	6.9300(14)	13.2864(2)	16.3434(2)
c (Å)	14.760(3)	7.2865(2)	12.5154(2)
V (Å^3)	2250.31	1286.27(5)	3342.95(10)
Z	4	2	8
Temperature (K)	293	297	297
Radiation type	synchrotron, λ = 0.7749 Å	Mo Kα, λ = 0.71073 Å	Mo Kα, λ = 0.71073 Å
F(000)	608	436.0	1136.0
Θ range (°)	1.81 – 27.71	4.336 - 59.492	4.984 - 59.472
μ (mm^{-1})	1.088	0.982	1.455
Reflections collected / unique (Rint)	8438/1637 (0.034)	14665/1001 (0.052)	22684/2204 (0.032)
Data/parameters	1637/54	1001/36	2204/79
GooF on F^2	1.206	1.10	1.13
Final R indices [I > 2 б(I)]	R_1 = 0.0660	R_1 = 0.0290	R_1 = 0.032
	wR_2 = 0.2120	wR_2 = 0.0848	wR_2 = 0.1179
Largest diff. peak / hole, eÅ^{-3}	0.790, -0.928	0.25, −0.27	0.54 −0.29

Kinetics of the esterification and equilibrium constant determination

To determine the rate constants k_1 and k_{-1} of the esterification, two sets of samples were prepared. For the first set with Ni^{2+} ions, 14 ml BuOH and 3.50 ml of AA were mixed with $Ni(NO_3)_2 \cdot 6H_2O$ (50 mg, 173 µmol). The mixture was sonicated until the metal salt dissolved. For the second catalyst-free set, 14 ml of BuOH and 3.5 ml of AA were mixed and sonicated along with the first sample set. From both mixtures, 1.5 ml was distributed into 11 dried scintillation tubes each. All Pyrex tubes except one, which is t = 0, were placed in a preheated oven at a specific temperature. Samples were removed from the oven at t = 0.5, 1, 2, 3, 4, 5, 6, 7, 8, and 24 h. The samples were cooled rapidly by placing them directly into a 4°C fridge. The procedure was carried out at T = 140 °C, 150 °C, and 160 °C.

The concentration of BuOH, AA, and BuOAc was determined from ^{1}H-NMR spectra. A benzene solution in DMSO-d6 was prepared with the benzene to serve as an internal NMR standard. The sample (50 µl) was diluted in 700 µl of the standard solution. The concentration of the reactants was determined by calculating the ratio of the reactant peak integral to that of the internal standard, benzene. When multiple proton signals of one substance could be analyzed, the average value for the molarity was chosen.

To validate the NMR results, three samples from each measured set taken at t = 0, 3, 6, or 8 h were analyzed by conductometric titration to determine the concentration of AA. The sample (500 µl) was diluted with DI water (1 ml) and titrated with 1 M NaOH under stirring.

The concentration of the formed water in the reactions could not be determined; therefore, it was estimated from the concentration of the formed ester and, if applicable, the crystal water of the nickel salt.

The concentration profiles over time were fitted with numerical fits using a dedicated Python script. [10]

$$\frac{d[BuOAc]}{dt} = k_1[AA][BuOH] - k_{-1}[BuOAc][H_2O] \quad (1)$$

$$\frac{d[BuOH]}{dt} = k_{-1}[BuOAc][H_2O] - k_1[AA][BuOH] \quad (2)$$

$$\frac{d[AA]}{dt} = k_{-1}[BuOAc][H_2O] - k_1[AA][BuOH] \quad (3)$$

$$[H_2O] = [BuOAc] + 6[Ni^{2+}] \quad (4)$$

For the determination of the equilibrium constant *K* again, two sets of samples, with and without Ni^{2+} ions, respectively, were prepared according to the procedure for the determination of the rate constants. The mixture of each set was distributed into 9 scintillation vials and sealed. Of each set, 3 scintillation vials with the reaction mixture were placed at T = 130, 150, and 170 °C, each. After 72 h, the samples were rapidly cooled in the fridge. All samples were analyzed using conductometric titration to determine the residual concentration of AA. The concentration of the water was estimated in the same manner as upon determination of the rate constants.

Reaction Kinetics of Esterification

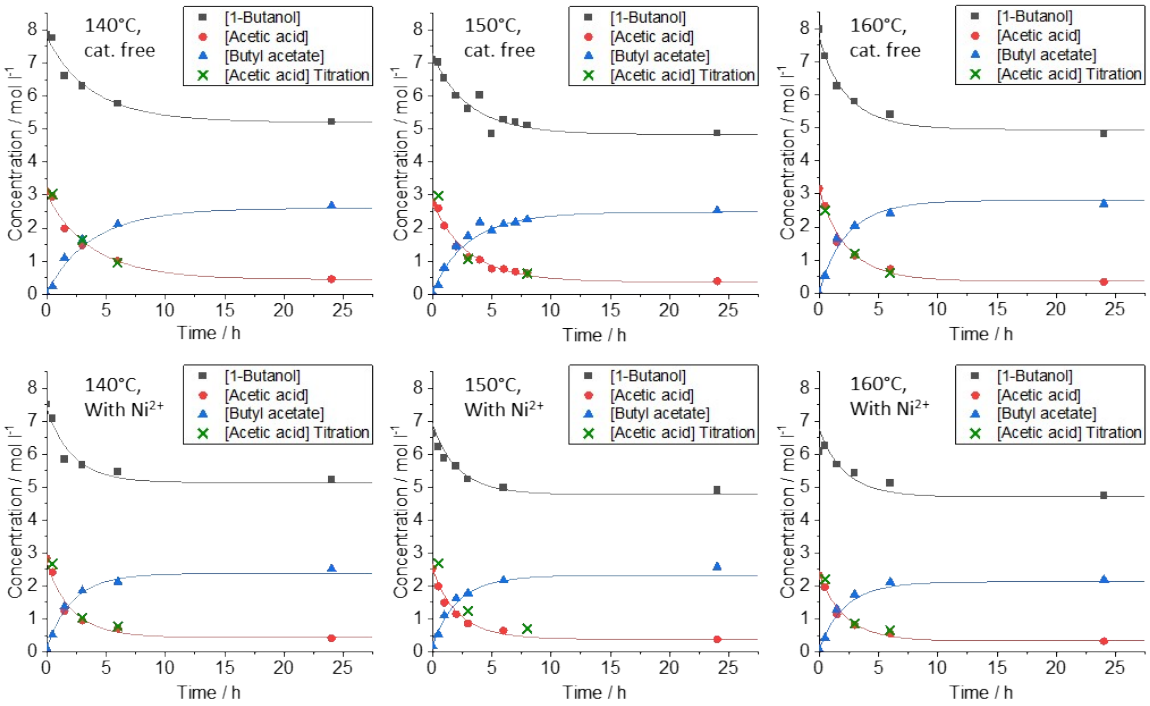

Figure S1. Experimentally measured concentration profiles of the esterification reaction at 140, 150, and 160 °C without catalyst (top row) and with Ni^{2+} as catalyst (bottom row) with numerically determined differential fits.

NMR

Table S4: Summary of the integrals of the NMR spectra from the esterification at 140°C in the presence of Ni^{2+} ions. In brackets behind the substance is the number of protons creating the signal given. The amount of the internal standard benzene is 0.165 mmol.

	Benzene (6H)	BuOH (3H)+ BuOAc (3H)	AA (3H)	BuOAc(2H)	BuOAc(3H)
δ / ppm Time / h	7.37	0.88	1.91	3.99	1.99
0	6	6.8976	2.5664	0.0633	0.0916
0.5	6	6.8934	2.1940	0.3063	0.4770
1.5	6	6.5504	1.1177	0.8262	1.2623
3	6	6.8000	0.8581	1.1378	1.6566
6	6	6.8625	0.6504	1.2987	1.9070
24	6	6.9638	0.3741	1.5496	2.2396

Table S5. Summary of the integrals of the NMR spectra from the esterification at 150°C in the presence of Ni^{2+} ions. In brackets behind the substance is the number of protons creating the signal given. The amount of the internal standard benzene is 0.166 mmol.

	Benzene (6H)	BuOH (3H)+ BuOAc (3H)	AA (3H)	BuOAc (2H)	BuOAc (3H)
δ / ppm / Time / h	7.37	0.88	1.91	3.99	1.99
0	6	6.0831	2.2650	0.1092	0.1533
0.5	6	6.0287	1.7839	0.3293	0.4587
3	6	6.2242	0.7728	1.1096	1.5342
6	6	6.3463	0.5771	1.3425	1.8755
24	6	6.6495	0.3391	1.5858	2.2380

Table S6. Summary of the integrals of the NMR spectra from the esterification at 160°C in the presence of Ni^{2+} ions. In brackets behind the substance is the number of protons creating the signal given. The amount of the internal standard benzene is 0,170 mmol.

	Benzene (6H)	BuOH (3H)+ BuOAc(3H)	AA (3H)	BuOAc(2H)	BuOAc(3H)
δ / ppm / Time / h	7.37	0.88	1.91	3.99	1.99
0	6	5.4050	2.0579	0.0296	0.0687
0.5	6	5.8132	1.7418	0.2814	0.3166
1.5	6	5.8585	1.0076	0.8326	1.0366
3	6	5.9213	0.7261	1.1123	1.4219
6	6	5.8950	0.4918	1.3593	1.6993
24	6	5.5248	0.2864	1.3369	1.8702

Table S7. Summary of the integrals of the NMR spectra from the esterification at 140 °C in the absence of Ni^{2+} ions. In brackets behind the substance is the number of protons creating the signal given. The amount of the internal standard benzene is 0.165 mmol.

	Benzene (6H)	BuOH (1H)	BuOH (3H)+ BuOAc (3H)	AA (1H)	AA (3H)	BuOAc (2H)	BuOAc (3H)
δ / ppm / Time / h	7.37	4.3	0.88	11.9	1.91	3.99	1.99
0	6	2.3082	7.3480	0.9108	2.9333	0.0113	0.0128
0.5	6	2.2790	7.4650	0.8714	2.7478	0.1446	0.2180
1.5	6	1.9448	7.1432	0.5878	1.8510	0.6815	0.9885
3	6	1.8502	7.3700	0.4258	1.4159	1.0061	1.4893
6	6	1.6798	7.3587	0.2835	0.9974	1.2917	1.9209
24	6	1.5153	7.3360	0.1193	0.4773	1.6320	2.4128

Table S8. Summary of the integrals of the NMR spectra from the esterification at 150 °C in the absence of Ni^{2+} ions. In brackets behind the substance is the number of protons creating the signal given. The amount of the internal standard benzene is 0.166 mmol.

	Benzene (6H)	BuOH (3H)+ BuOAc (3H)	AA (3H)	BuOAc (2H)	BuOAc (3H)
δ / ppm / Time / h	7.37	0.88	1.91	3.99	1.99
0	6	6.4568	2.4970	0.0313	0.0400
0.5	6	6.6047	2.3630	0.1712	0.2407
1	6	6.6375	1.8847	0.4954	0.7192
2	6	6.7499	1.3206	0.8978	1.3054
3	6	6.6544	1.0195	1.0769	1.5710
4	6	7.3979	0.9521	1.3415	1.9430
5	6	6.1294	0.6990	1.1728	1.7224
6	6	6.7039	0.6963	1.2866	1.9200
7	6	6.7080	0.6236	1.3061	1.9847
8	6	6.6745	0.5750	1.3755	2.0357
24	6	6.6590	0.3604	1.5645	2.2427

Table S9. Summary of the integrals of the NMR spectra from the esterification at 160°C in the absence of Ni^{2+} ions. In brackets behind the substance is the number of protons creating the signal given. The amount of the internal standard benzene is 0,165 mmol.

	Benzene (6H)	BuOH (1H)	BuOH (3H)+ BuOAc(3H)	AA (3H)	BuOAc(2H)	BuOAc(3H)
δ / ppm / Time / h	7.37	4.3	0.88	1.91	3.99	1.99
0	6	2.3810	7.3160	2.8637	0.0085	0.0093
0.5	6	2.0818	7.2169	2.3921	0.3241	0.4781
1.5	6	1.8445	7.3350	1.3963	1.0138	1.5019
3	6	1.7072	7.2248	1.0321	1.2465	1.8340
6	6	1.5743	7.2408	0.6648	1.4833	2.1655
24	6	1.3635	6.9891	0.3106	1.6731	2.3821

Conductometric Titration

Table S10. Concentration of AA in mol l^{-1} in different samples of the esterification in the presence of Ni^{2+} determined by conductometric titration.

time / h / T/ °C	0.5	3	6
140	2.6719	1.0354	0.7737
150	2.7210	1.27035	0.73118*
160	2.2054	0.87186	0.66034

* The concentration of AA was determined after 8 h instead of 6 h.

Table S11. Concentration of AA in mol l^{-1} in different samples of the esterification in the absence of Ni^{2+} determined by conductometric titration.

T/ °C \ time / h	0.5	3	6
140	3.0310	1.6430	0.9619
150	2.9854	1.0714	0.6264*
160	2.5072	1.2000	0.6191

* The concentration of AA was determined after 8 h instead of 6 h.

Determination of the esterification equilibrium K

Conductometric Titration

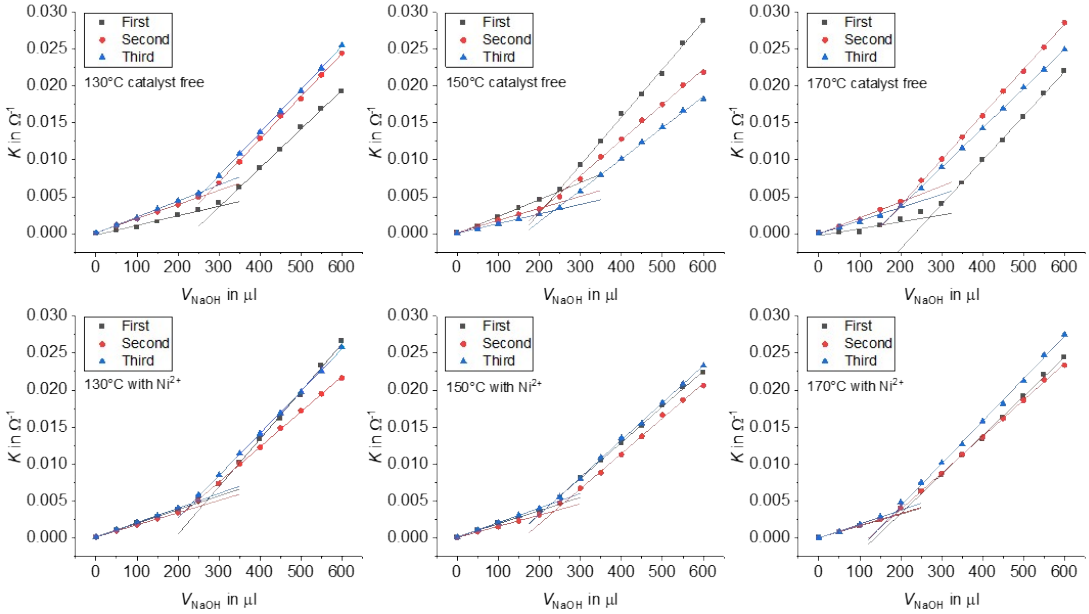

Figure S2. Conductometric titrations of the esterification reactions at equilibrium.

Table S12. Concentration of AA in mol L^{-1} in different samples of the esterification in the presence of Ni^{2+} determined by conductometric titration.

sample \ T/ °C	130	150	170
1	0.5395	0.4355	0.3822
2	0.4603	0.4603	0.3623
3	0.5052	0.4610	0.3608
Average	0.5016	0.4523	0.3684

Table S13: Concentration of AA in mol L^{-1} in different samples of the esterification in the absence of Ni^{2+} determined by conductometric titration.

T/ °C / sample	130	150	170
1	0.5929	0.48934	0.5640*
2	0.5482	0.43804	0.4011
3	0.5313	0.47992	0.3769
Average	0.5575	0.4691	0.3890

* The concentration was not used for the calculation of the average concentration.

Predicted concentration evolution profiles in the BuOH+AA DSS

From the linear dependence of ln(k_1) vs. T and ln(K) vs. T both kinetic rate constants k_1 and k_{-1} were determined. The values were utilized to perform numerical fits with the chemical-kinetics Python module for different initial AA concentrations between 0 and 4.35 mol/l as employed in the syntheses.[10] The calculated AA concentrations show a rapid decline within the first 5 h and a plateau afterward. The progress of the esterification can also be monitored by the decrease of the BuOH content. The amount of 1-butanol consumed is expressed as a percentage of its initial concentration.

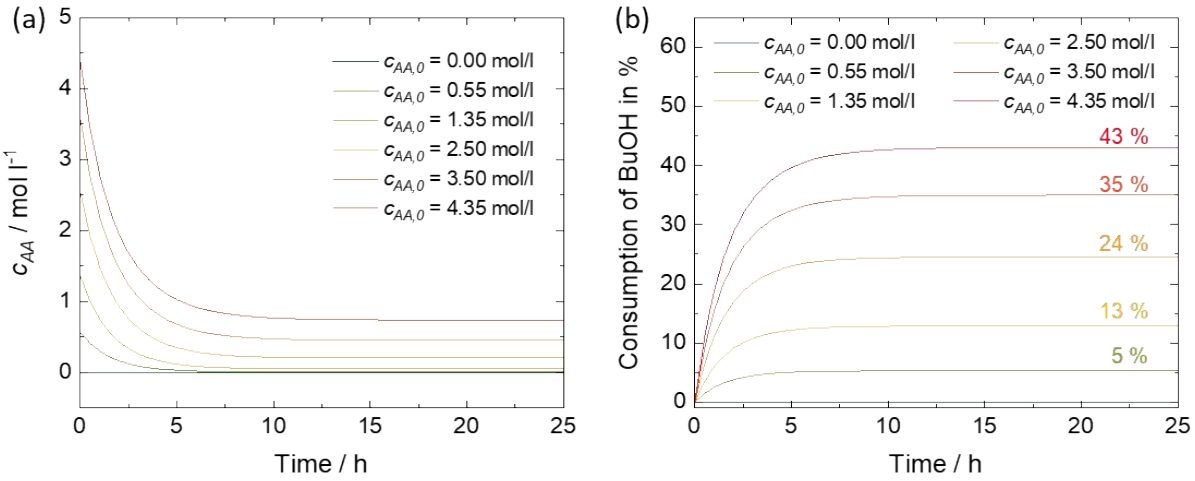

Figure S3. Calculated concentration profile of AA (a) and consumption of BuOH (b) in a **NiBDP$_{B+AA}$** synthesis at 150 °C (323 K).

TGA/DTA analysis

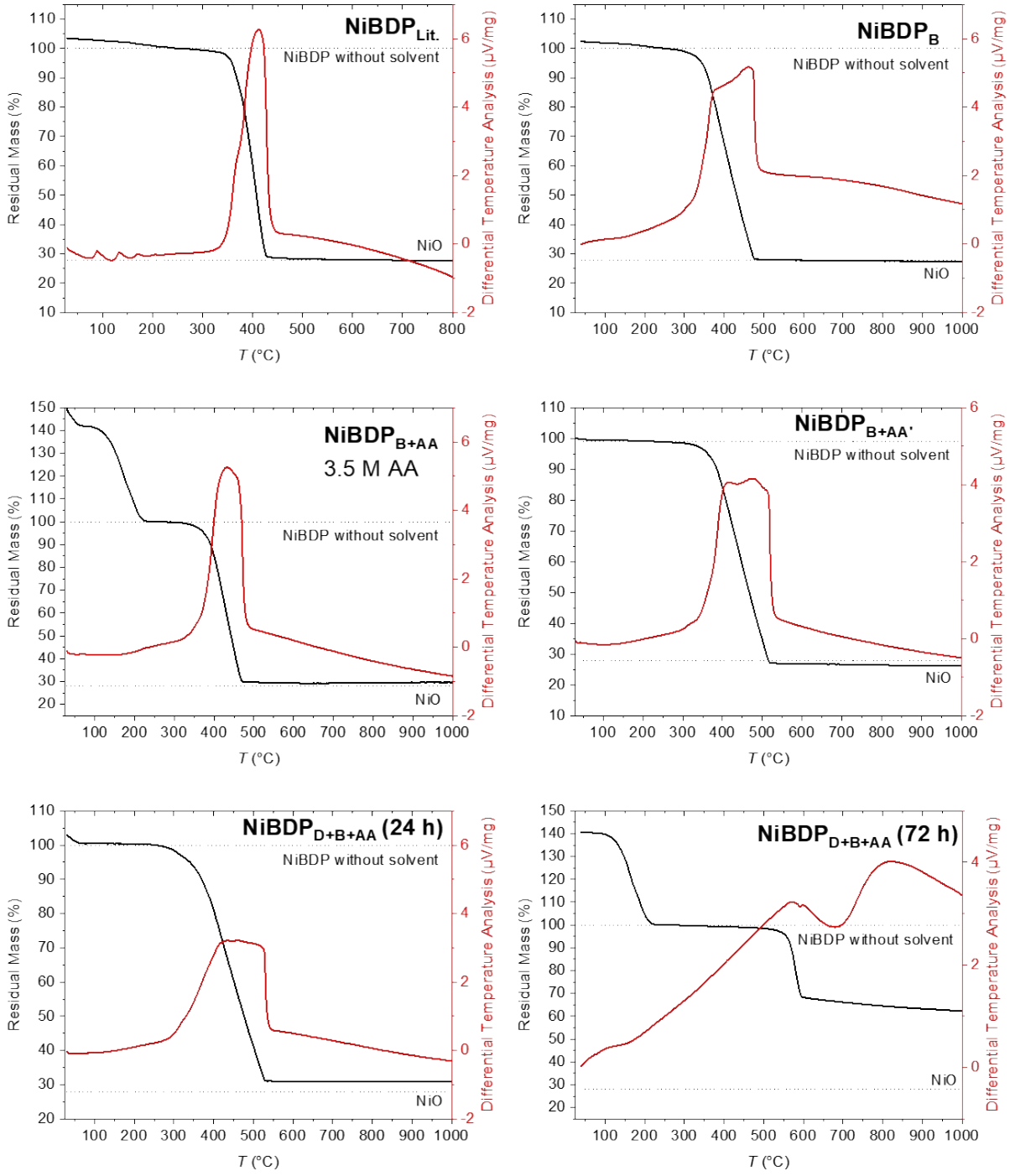

Figure S4. TGA/DTA analysis of relevant **NiBDP** samples normalized to the mass of the desolvated material and the calculated ideal residual mass of NiO.

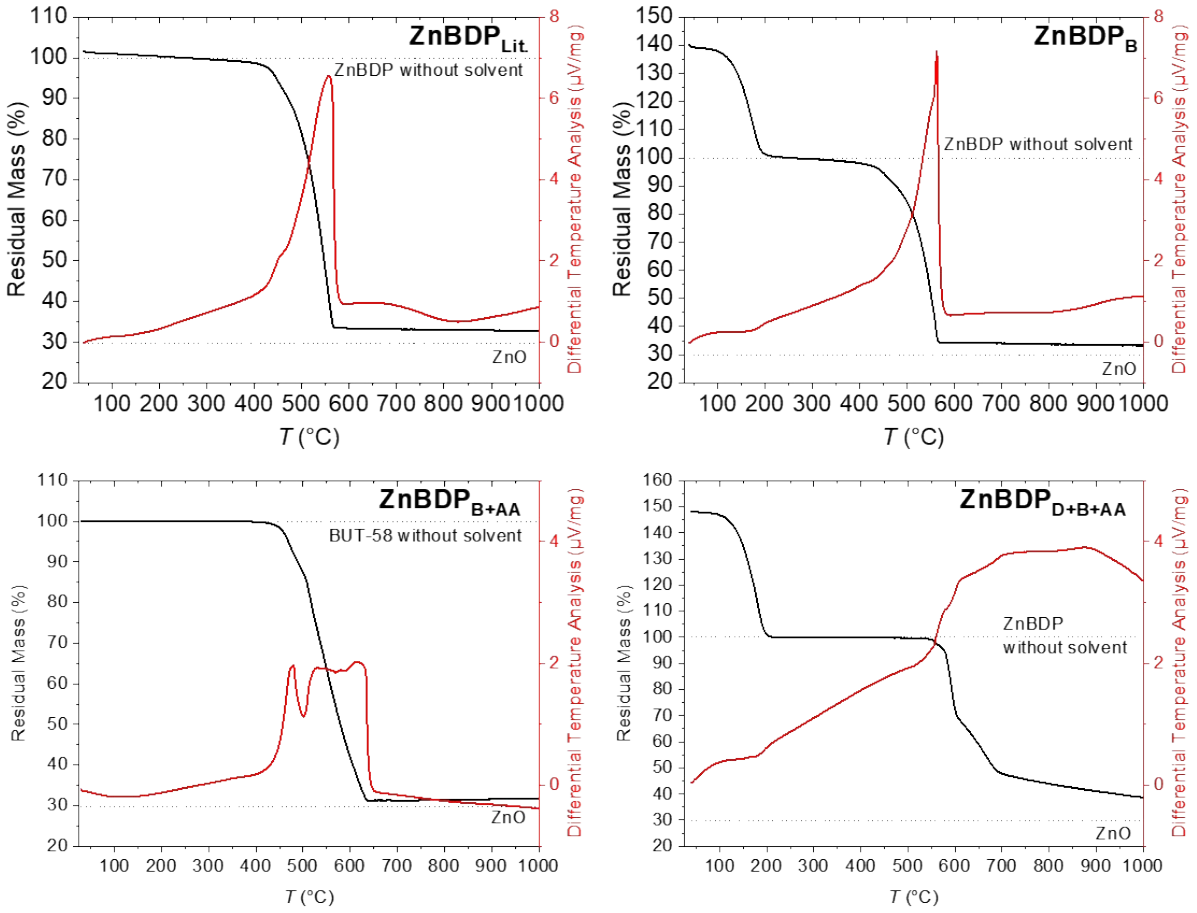

Figure S5. TGA/DTA analysis of relevant ZnBDP samples normalized to the mass of the desolvated material and the calculated ideal residual mass of ZnO.

From the ideal composition of the three investigated materials, which is one bdp linker per metal ion (*e.g.,* $C_{12}H_8N_4Ni$ for $[Ni(bdp)]_n$ and $C_{12}H_8N_4Zn$ for $[Zn(bdp)]_n$ and BUT-58, respectively), the theoretical metal oxide residual mass after combustion was calculated to be 27.98% for $[Ni(bdp)]_n$ and 29.74% for $[Zn(bdp)]_n$ and BUT-58. The samples **NiBDP$_{B+AA}$**, **NiBDP$_{D+B+AA}$ (72h)**, **ZnBDP$_{B}$**, and **ZnBDP$_{D+B+AA}$** were measured after washing with NMP/DMF but prior to activation. All other samples were measured after adsorption measurements. For the non-activated samples, the loss of solvent is clearly visible in the range from rt to 200 °C. The mass of the fully desolvated MOF is determined at 250 °C, and the TGs are normalized to this mass. For all samples, except for **ZnBDP$_{D+B+AA}$**, the combustion of the framework occurs at approx. 400 °C. The **ZnBDP$_{D+B+AA}$** only combusts at above 550 °C, which can be explained by the exceptionally large crystal size in this sample. Only two samples, **NiBDP$_{D+B+AA}$ (72h)** and **ZnBDP$_{D+B+AA}$**, demonstrate considerable deviations of the observed residual mass from the theoretical value. While for **ZnBDP$_{D+B+AA}$**, a longer incineration time may have been necessary to combust the sample completely, the **NiBDP$_{D+B+AA}$ (72h)** clearly contains a higher-than-expected amount of inorganic material, which we believe is an amorphous nickel formate.

Additional PXRD data

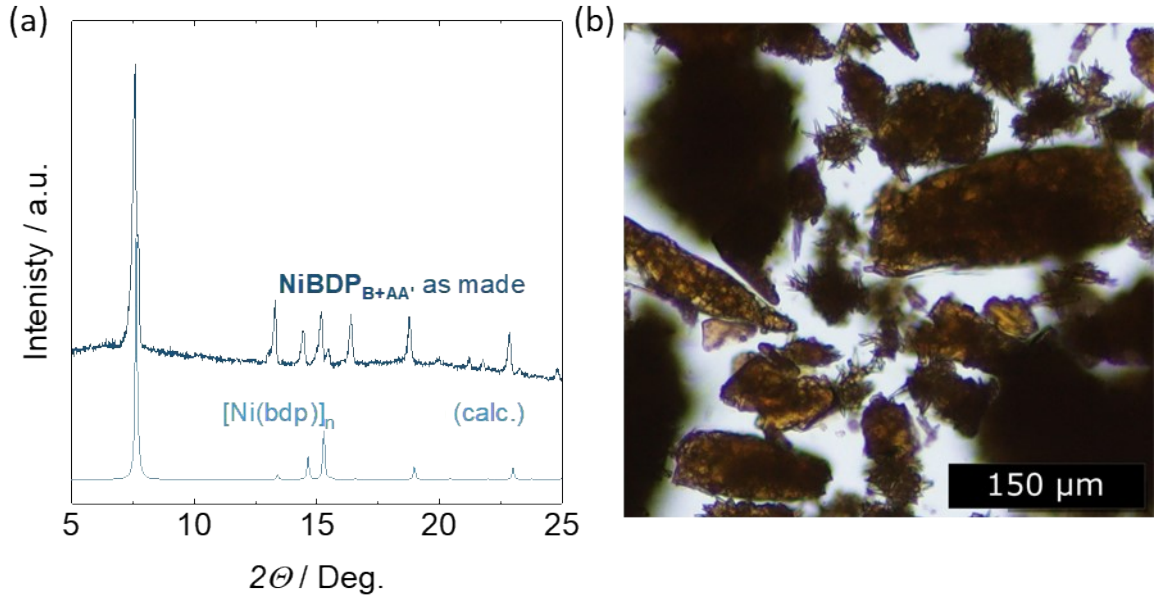

Figure S6. (a) PXRD patterns and (b) VLM of **NiBDP$_{B+AA}$***.

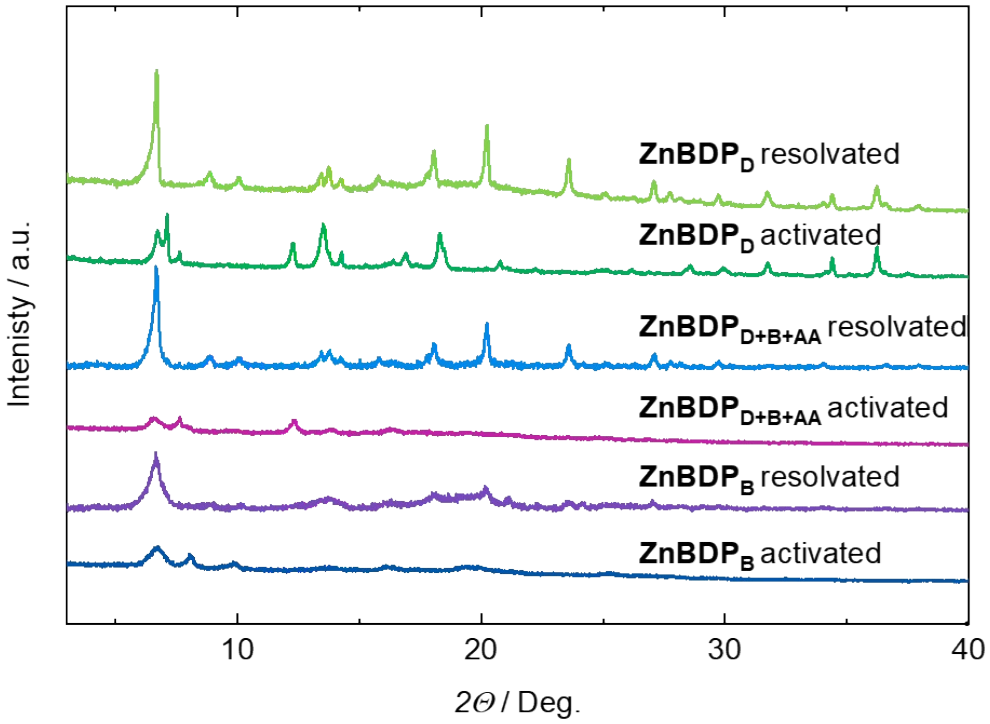

Figure S7. PXRD patterns of relevant ZnBDP samples after desolvation at 180 °C (4 h) and subsequent resolvation in DMF (1 h).

During desolvation, the material undergoes a solid-state structural transition, losing perfect crystalline order. Such amorphisation is commonly observed in flexible MOFs and does not necessarily indicate material degradation. The material recovers its crystallinity after resolvation and shows full adsorption capacity in adsorption experiments (Table S14 and S15). Thus, this loss of crystallinity upon activation has no detrimental impact on the adsorption performance.

Crystal size distributions

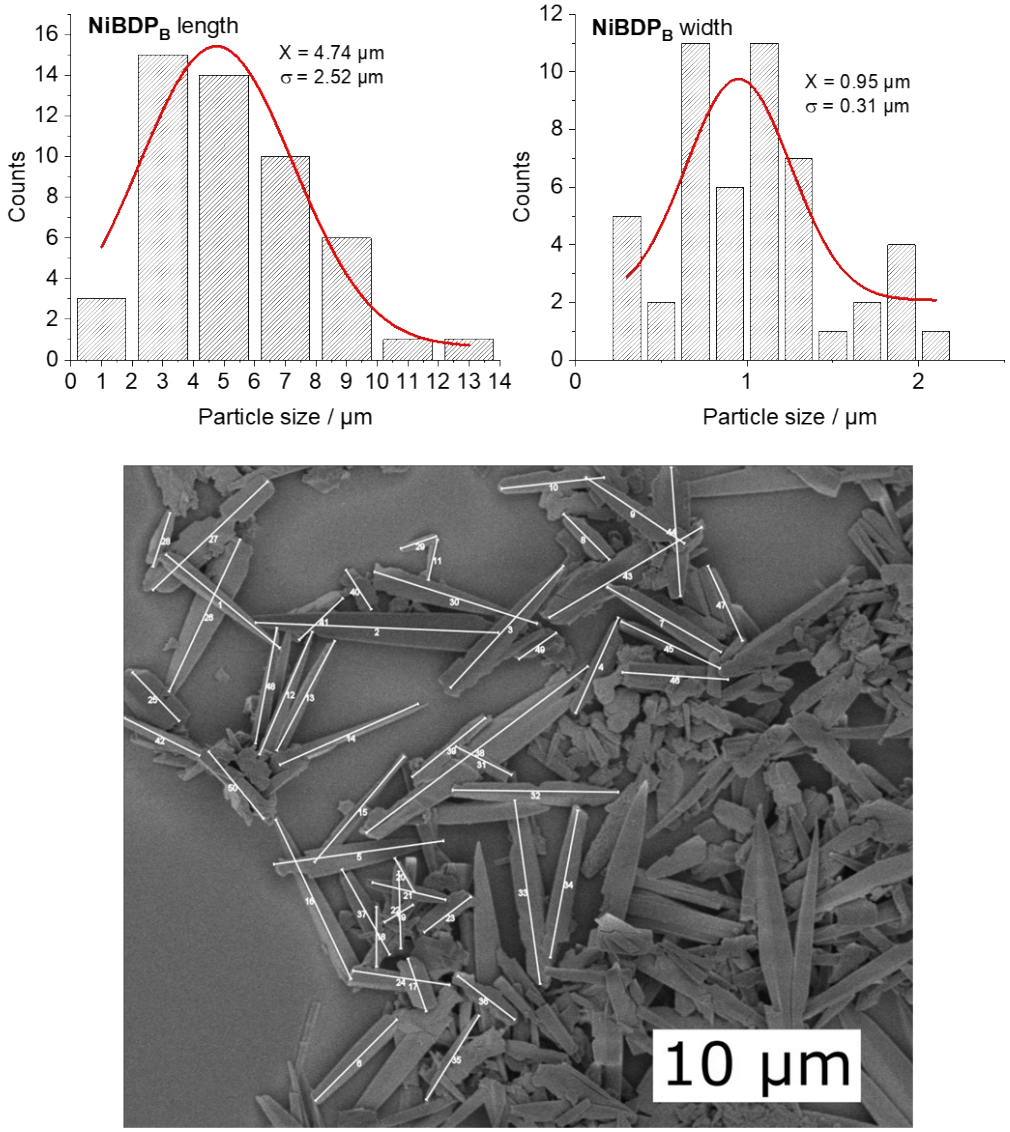

Figure S8. Histograms of the length and width distributions of the **NiBDP$_B$** crystals with a representative SEM image.

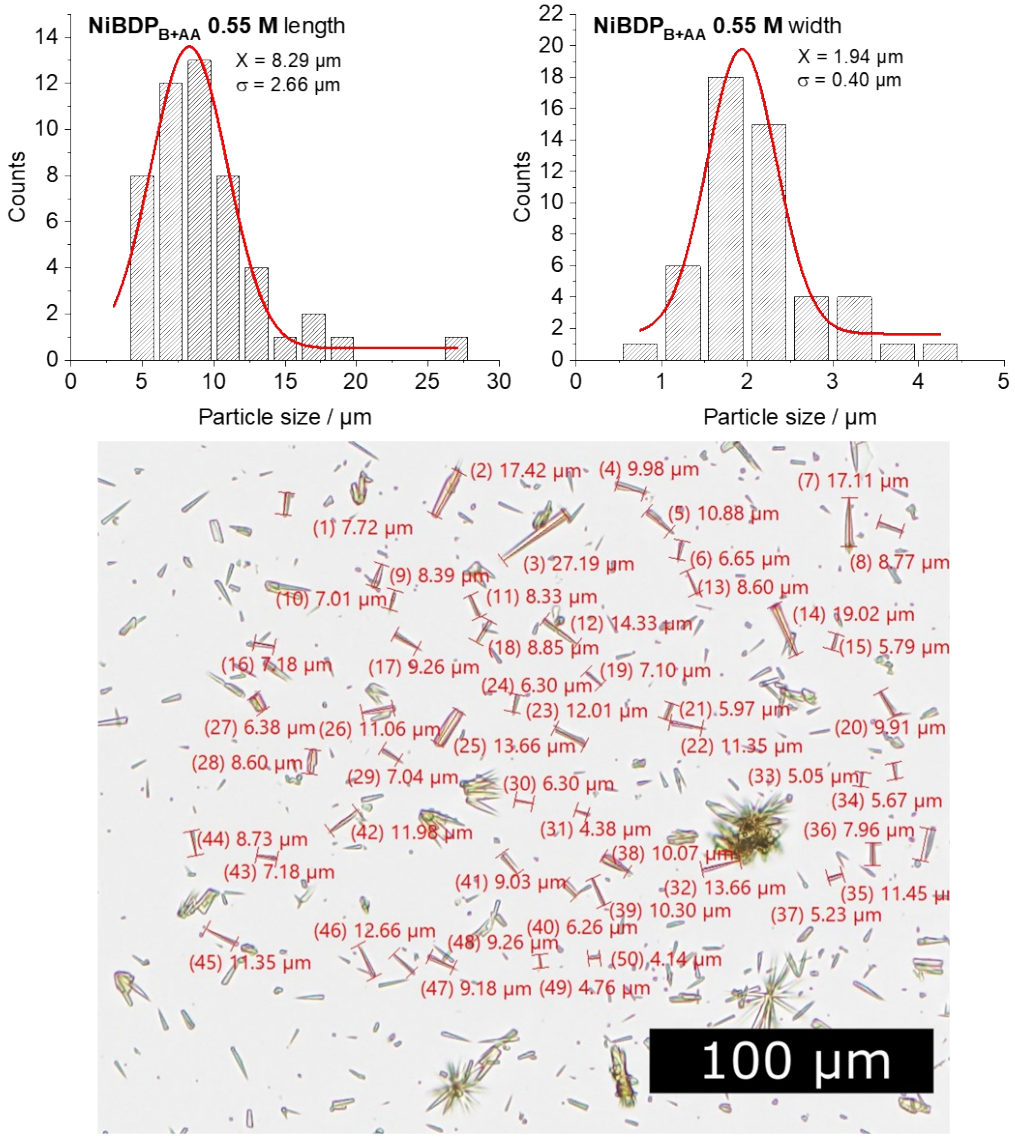

Figure S9. Histograms of the length and width distributions of the **NiBDP$_{B+AA}$** 0.55 M crystals with a representative VLM image.

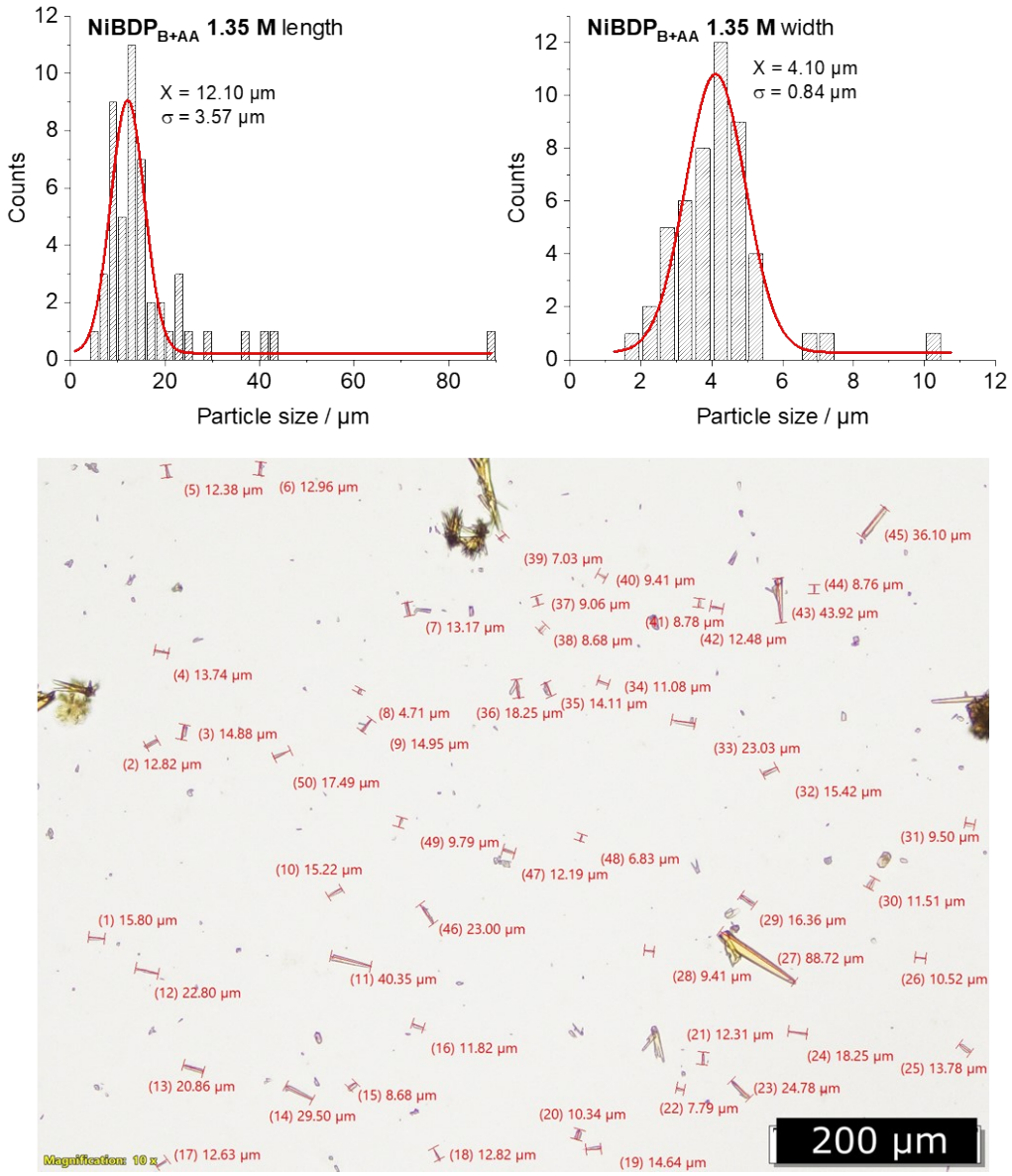

Figure S10. Histograms of the length and width distributions of the **NiBDP$_{B+AA}$** 1.35 M crystals with a representative VLM image.

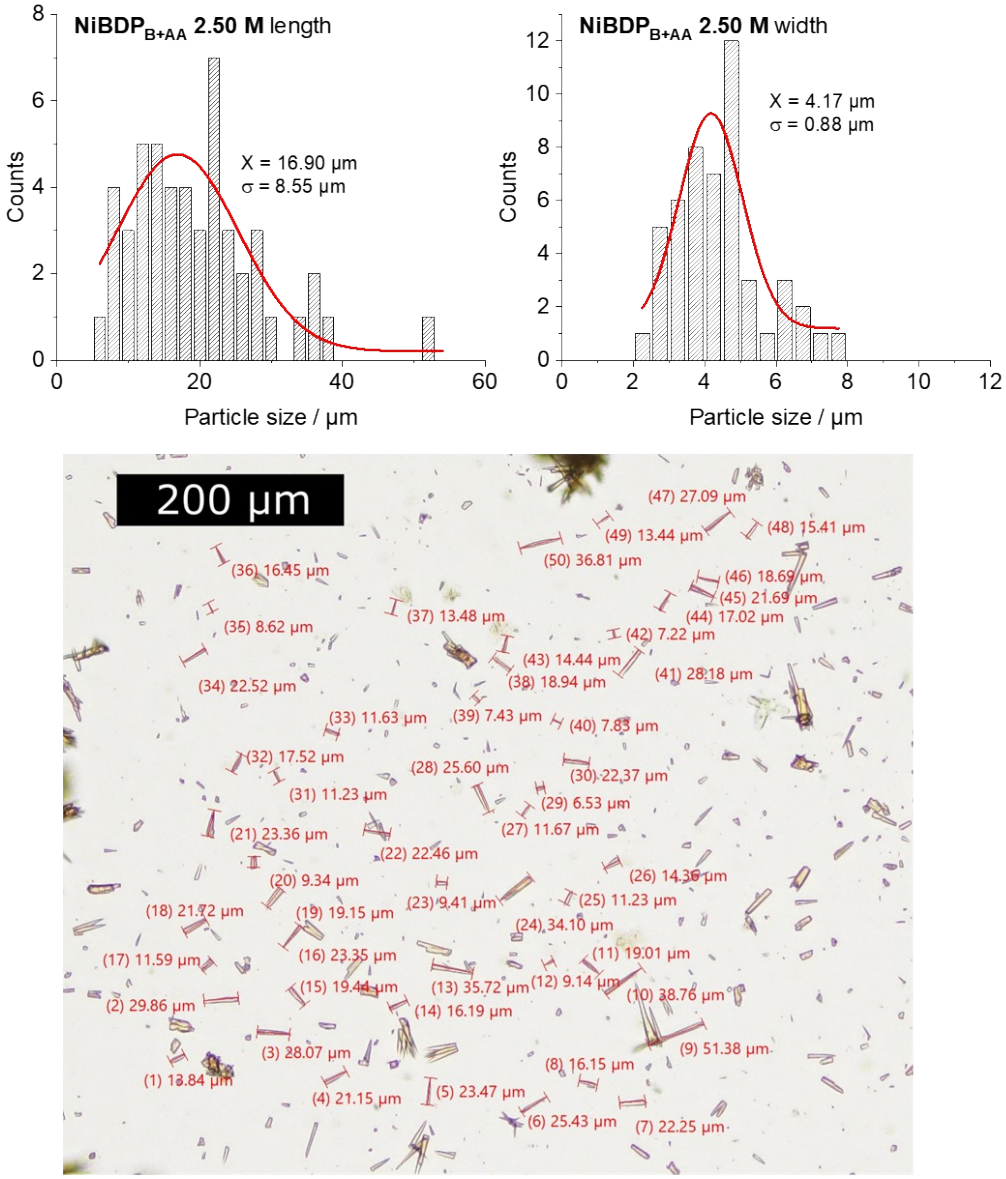

Figure S11. Histograms of the length and width distributions of the **NiBDP$_{B+AA}$** 2.50 M crystals with a representative VLM image.

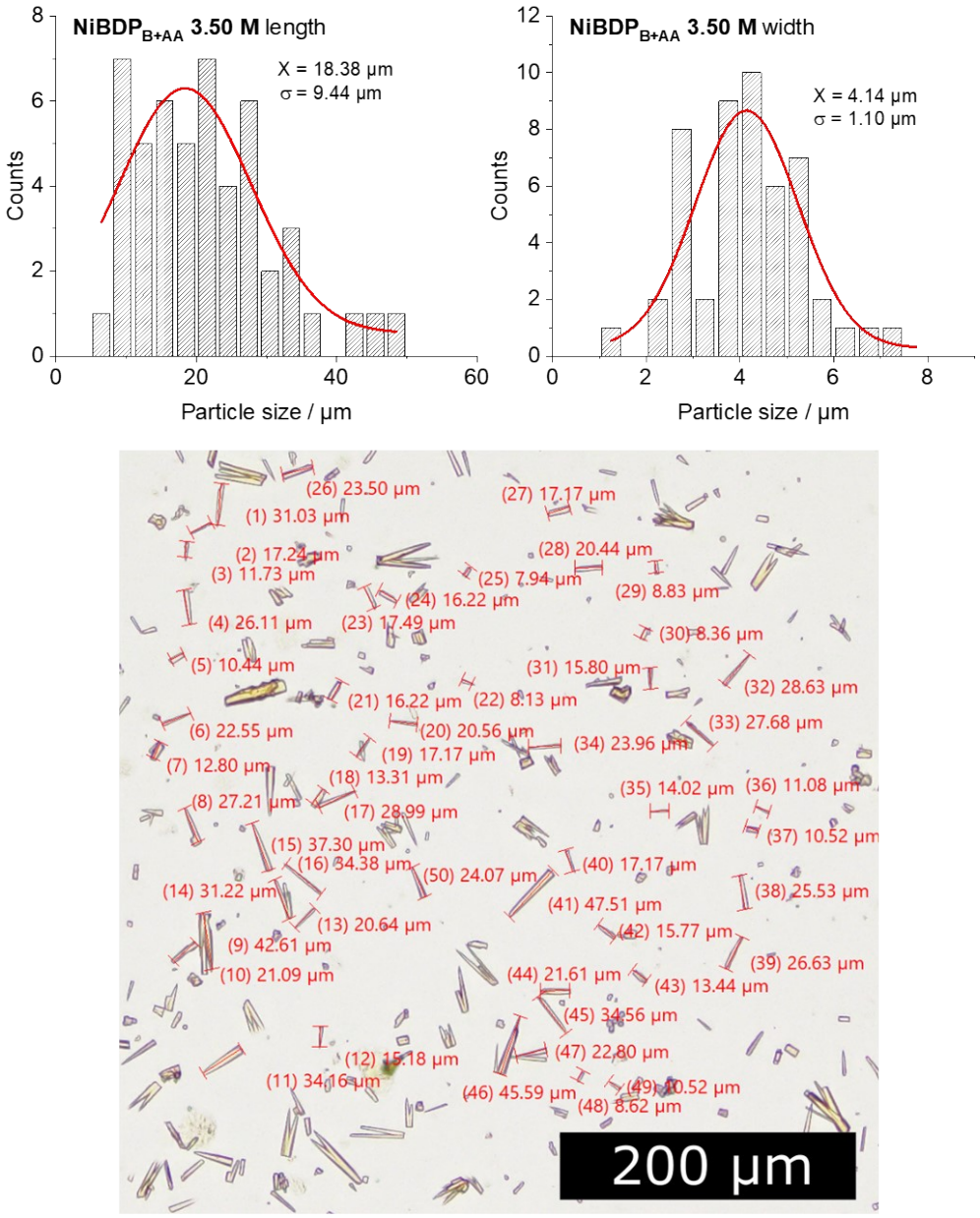

Figure S12. Histograms of the length and width distributions of the **NiBDP$_{B+AA}$** 3.50 M crystals with a representative VLM image.

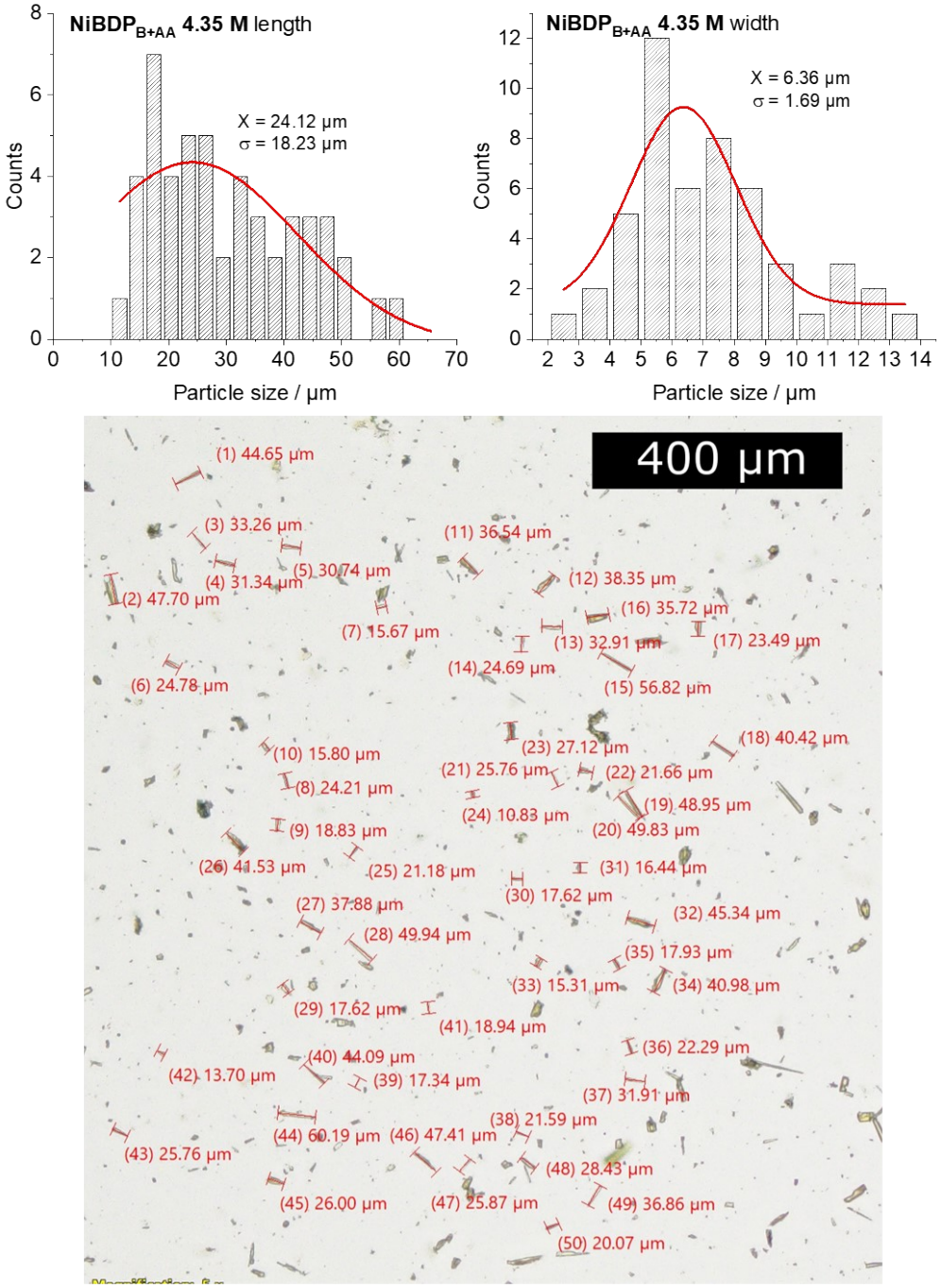

Figure S13. Histograms of the length and width distributions of the **NiBDP$_{B+AA}$** 4.35 M crystals with a representative VLM image.

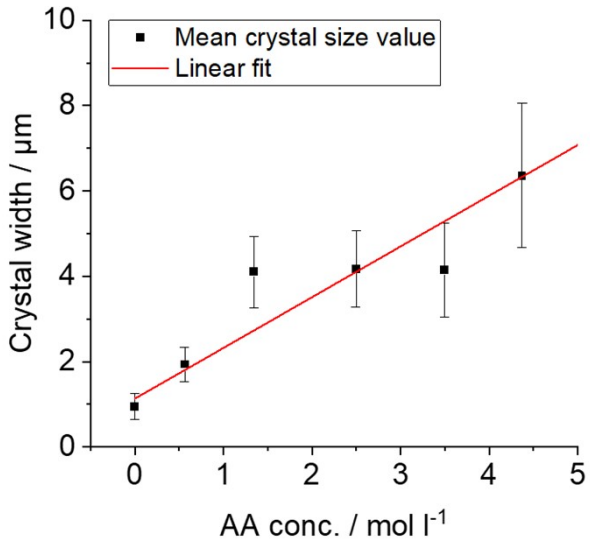

Figure S14. Increase in average crystal width of the **NiBDP$_{B+AA}$** with the rising amount of utilized AA.

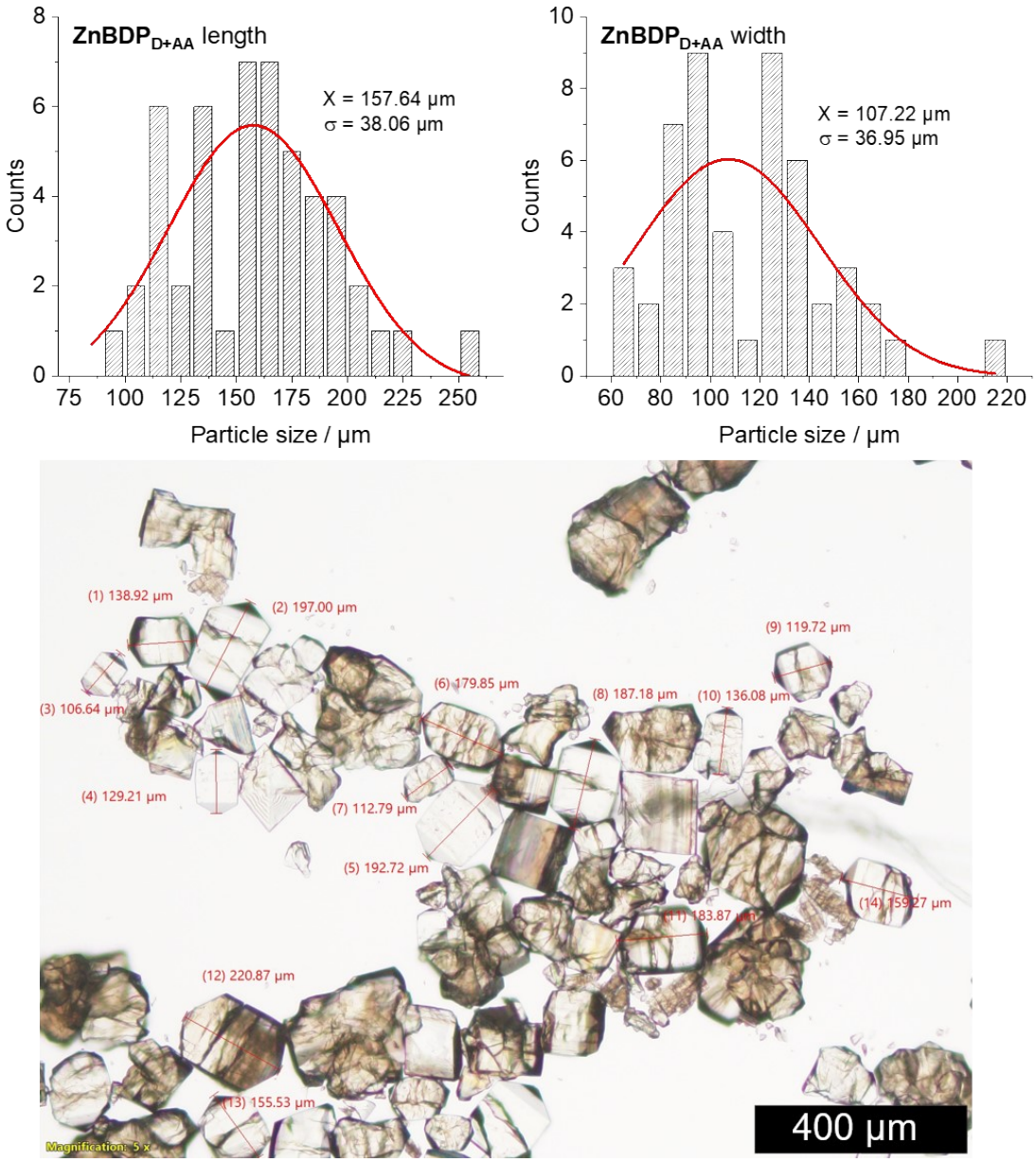

Figure S15. Histograms of the length and width distributions of the **ZnBDP$_{D+AA}$** crystals with a representative VLM image.

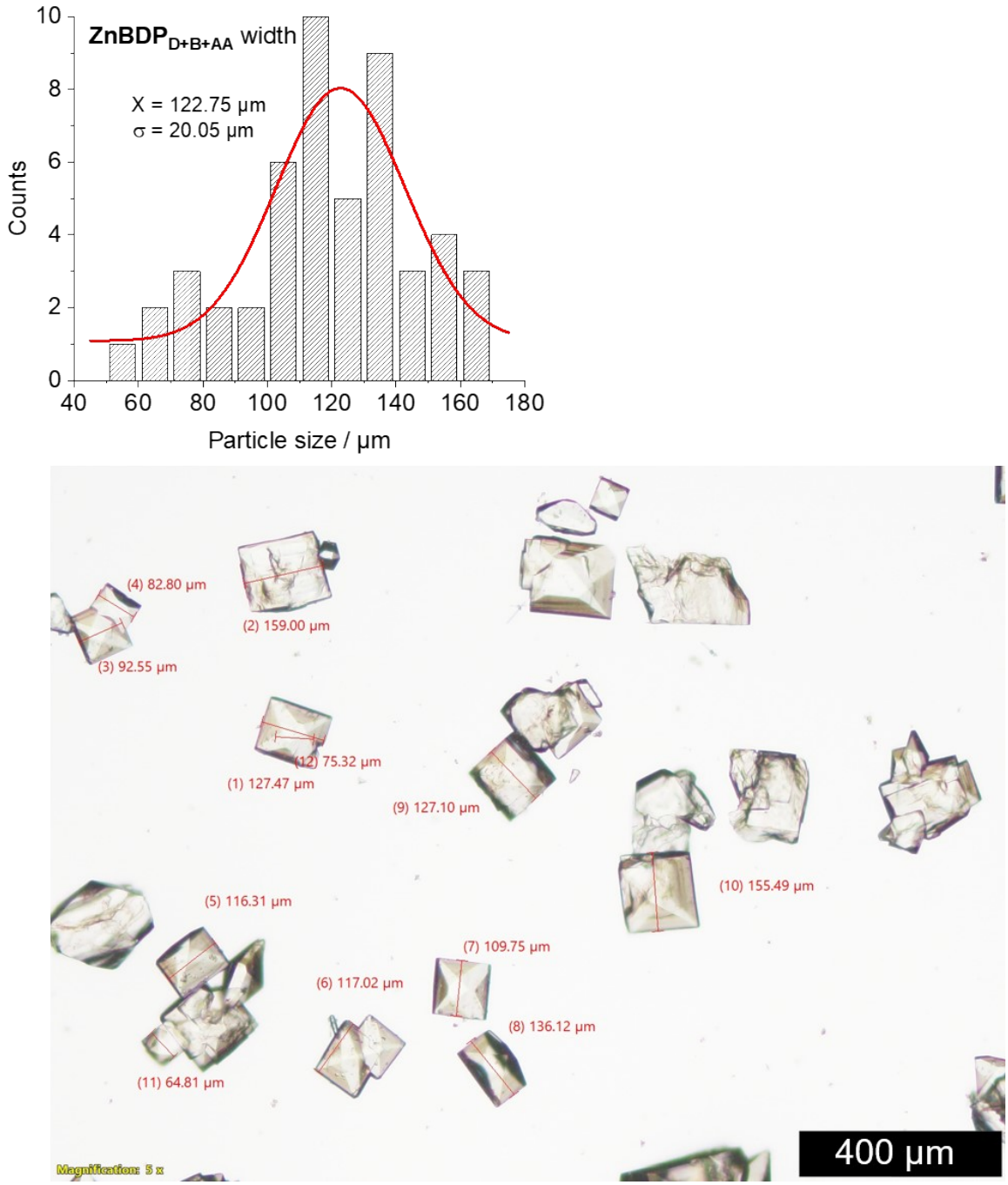

Figure S16. Histograms of the length and width distributions of the **ZnBDP$_{D+B+AA}$** crystals with a representative VLM image.

Pawley Refinement

For Pawley refinement, the most crystalline samples were chosen, all synthesized with a DSS approach.

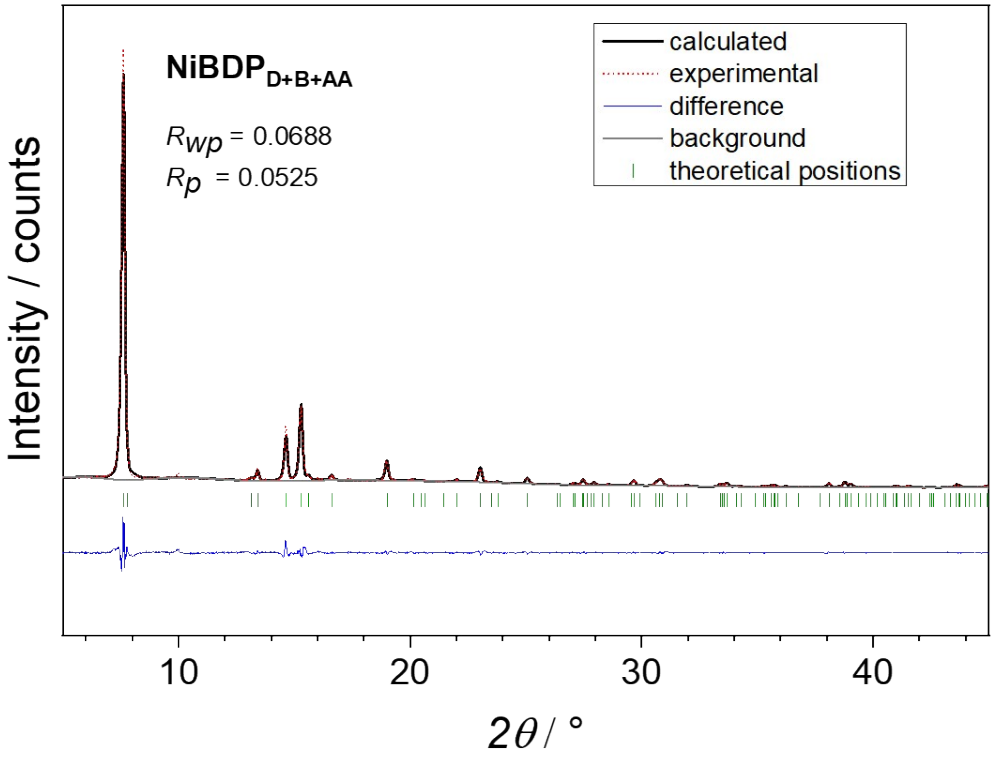

Figure S17. Pawley refinement of the activated **NiBDP$_{D+B+AA}$** sample after washing with DMF/NMP. Parameters of the refined cell: *Imma*; **a** = 6.7630 Å; **b** = 22.6822 Å; **c** = 13.4558 Å; V = 2064.12 Å^3.

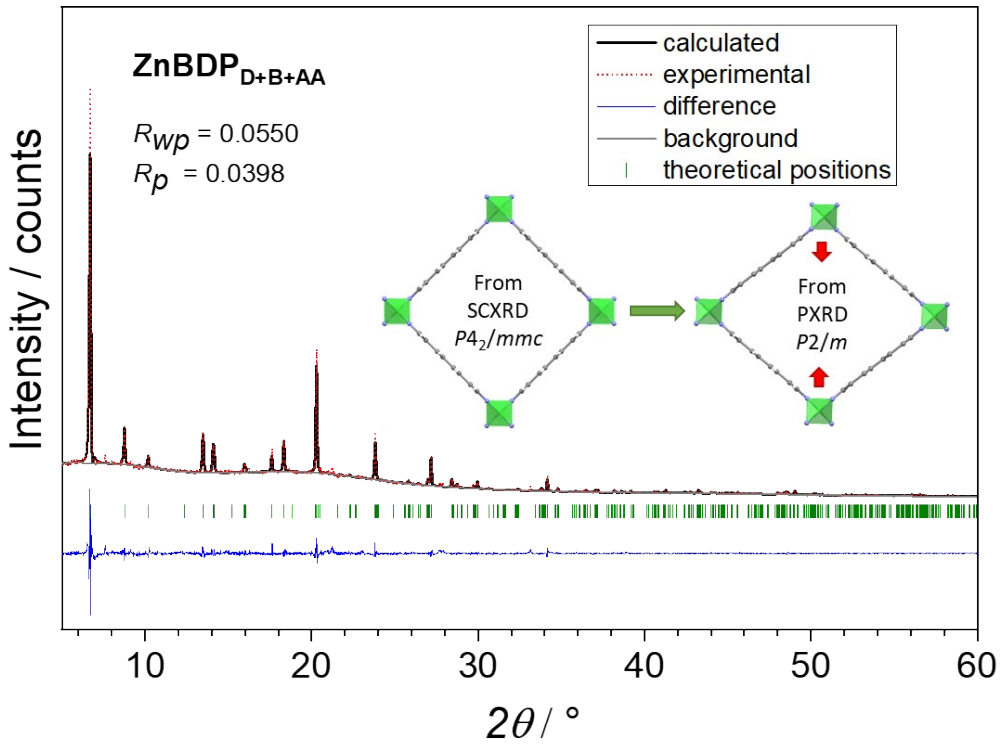

Figure S18. Pawley refinement of the solvated **ZnBDP$_{D+B+AA}$** sample after washing with DMF/NMP. Parameters of the refined cell: *P 2/m*; **a** = 13.2934 Å; **b** = 7.1476 Å; **c** = 13.2588 Å; V = 1245.69 Å^3.

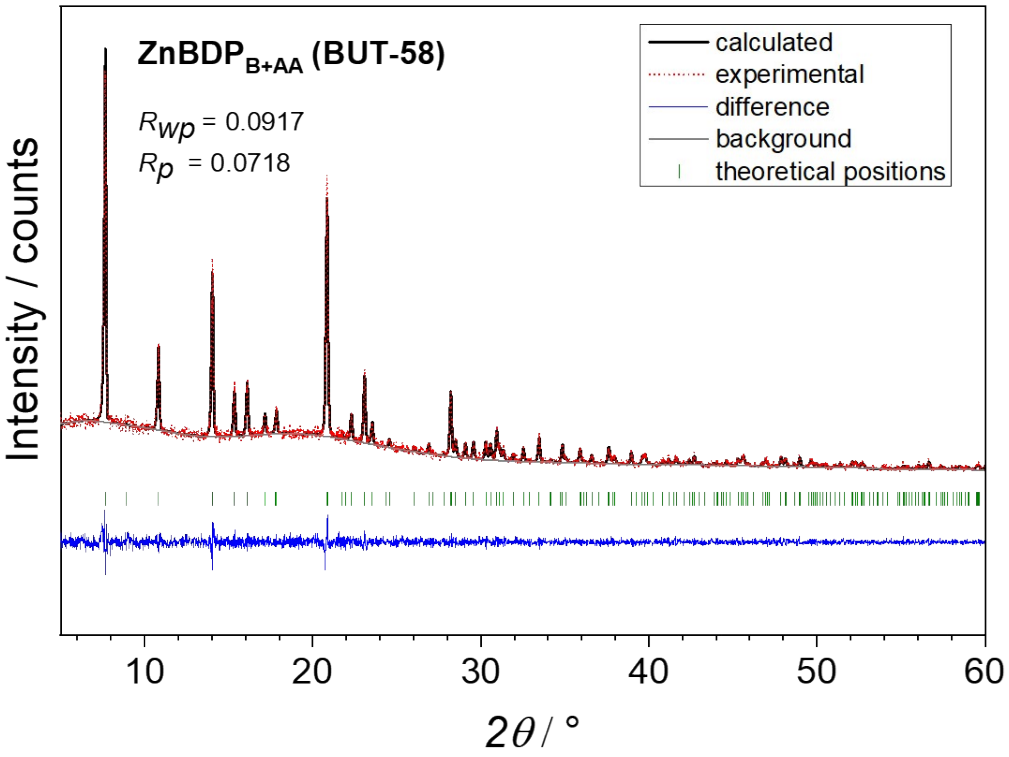

Figure S19. Pawley refinement of the activated **ZnBDP$_{B+AA}$** sample after washing with DMF/NMP. Parameters of the refined cell: *I* 4_1 *2 2*; **a** = 16.3332 Å; **b** = 16.3332 Å; **c** = 12.5120 Å; V = 3337.87 Å^3.

The Pawley refinement suggests a partial closing of the [Ni(bdp)]$_n$ and [Zn(bdp)]$_n$ phases during PXRD measurement, while the rigid BUT-58 phase remains the same. For [Zn(bdp)]$_n$ the closing of the pore results in a change of the space group from the *P*4_2/*mmc* to the lower symmetry *P 2/m*. This small change causes a pronounced shift of the reflections in the PXRD. The same effect also takes place for the [Ni(bdp)]$_n$ phase, although less pronounced. Thus, it is evident that it is difficult to measure a PXRD pattern for the two flexible phases which matches the single crystal structure perfectly, as the sample treatment required for PXRD measurement can induce a change of the cell opening state for example due to a partial loss of adsorbed solvent.

Additional Adsorption Data

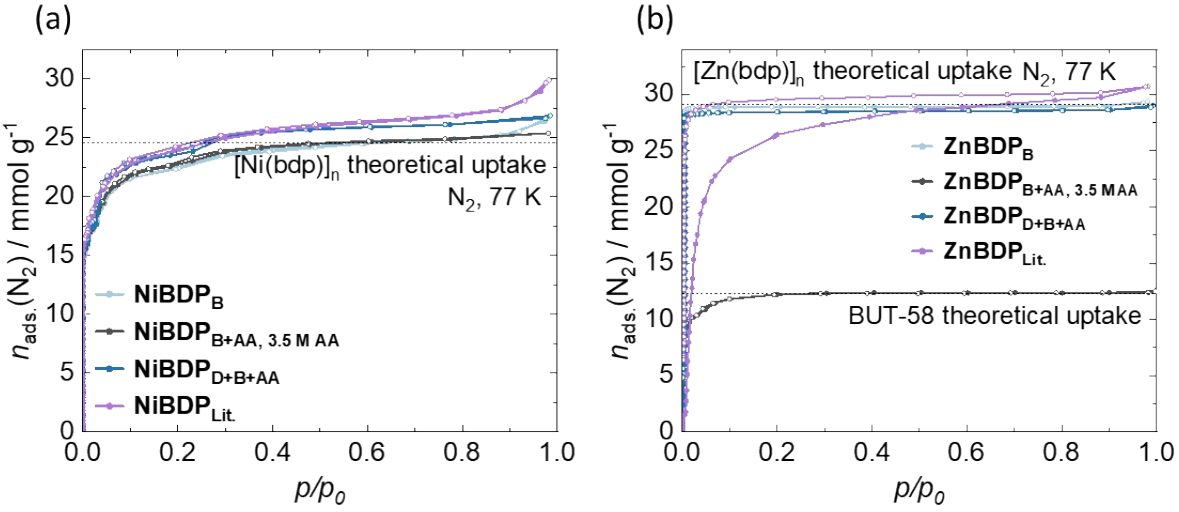

Figure S20. Linear scale nitrogen physisorption at 77 K of (a) $[Ni(bdp)]_n$ and (b) $[Zn(bdp)]_n$ from different syntheses washed with NMP/DMF, with theoretical uptakes of the corresponding phases indicated as dashed lines. Adsorption – filled symbols, desorption – open symbols.

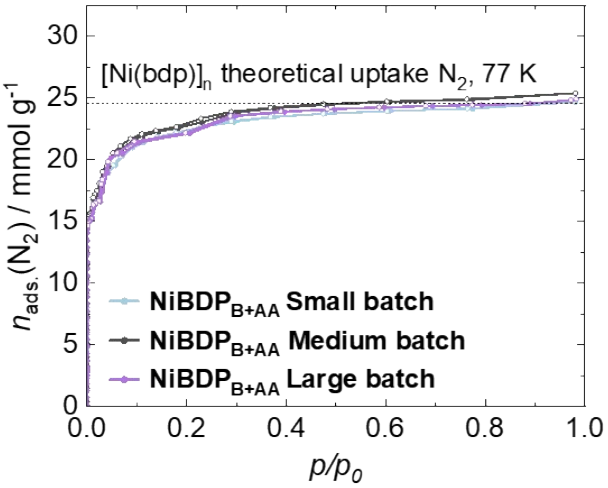

Figure S21. Linear scale nitrogen physisorption at 77 K of **NiBDP$_{B+AA}$** 3.5 M AA from differently sized synthetic batches washed with NMP/DMF, with the theoretical uptake indicated as a dashed line. Small batch – 10.7 mg H_2bdp + 14.8 mg $Ni(NO_3)_2{\cdot}6H_2O$. Medium batch – 53.5 mg H_2bdp + 74.0 mg $Ni(NO_3)_2{\cdot}6H_2O$. Large batch – 267.5 mg H_2bdp + 370.0 mg $Ni(NO_3)_2{\cdot}6H_2O$. Adsorption – filled symbols, desorption – open symbols.

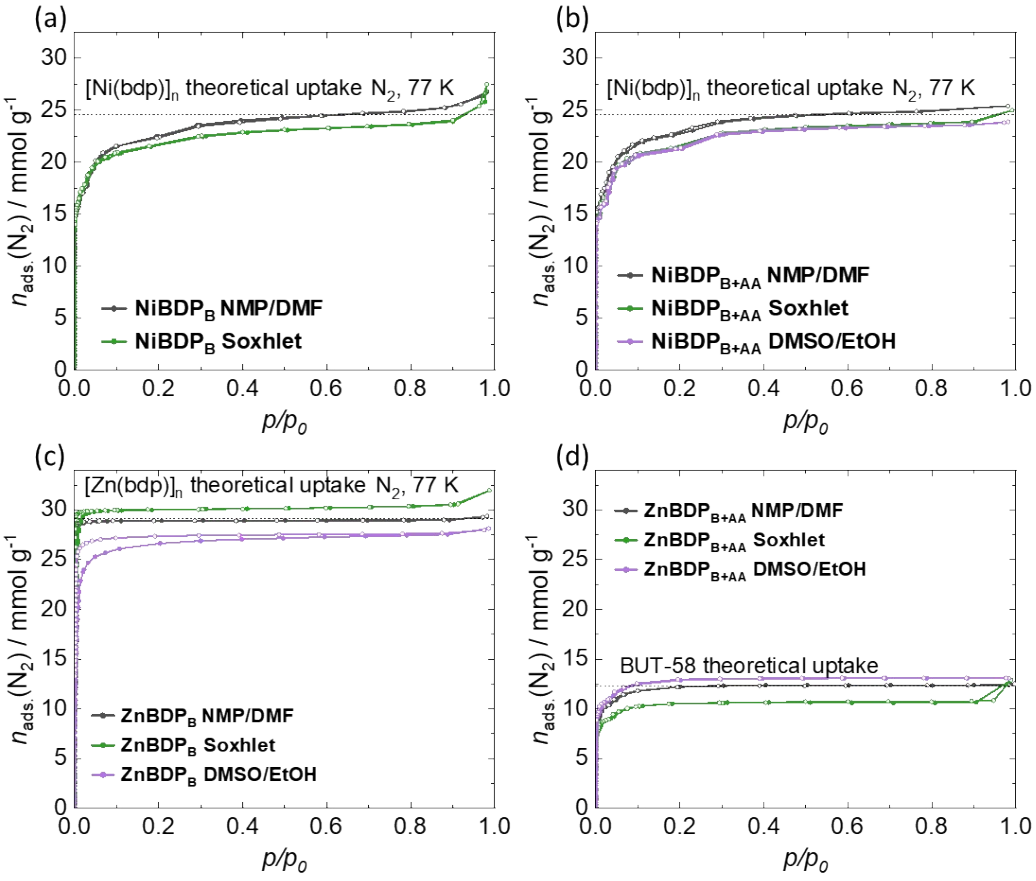

Figure S22. Nitrogen physisorption at 77 K shown in linear scale: (a) **NiBDP$_B$**, (b) **NiBDP$_{B+AA}$** 3.5 M AA, (c) **ZnBDP$_B$**, (d) **ZnBDP$_{B+AA}$** washed according to the general procedure (NMP/DMF) and compared to the materials washed with one or both sustainable washing methods (DMSO/EtOH) or (BuOH Soxhlet). Theoretical uptakes are indicated as dashed lines. Adsorption – filled symbols, desorption – open symbols.

The pore volumes of synthesized materials were compared to literature reported and to values calculated on the basis of crystallographic data. The pore volumes for all materials were determined from the nitrogen adsorption isotherms at 77 K at a p/p_0 = 0.8. Due to the lack of numerical adsorption data in the reported isotherms, the datapoints were extracted from the published isotherm images, which may result in lower accuracy.

Table S14. Pore volumes of **[Ni(bdp)]$_n$** samples derived from nitrogen physisorption at 77 K.

[Ni(bdp)]$_n$	
Material and washing procedure	**Pore Volume in cm^3/g**
NiBDP$_B$ NMP/DMF	0.861
NiBDP$_B$ Soxhlet	0.820
NiBDP$_{BA}$ NMP/DMF	0.861
NiBDP$_{BA}$ DMSO/EtOH	0.823
NiBDP$_{BA}$ Soxhlet	0.814
NiBDP$_{DBA}$ NMP/DMF	0.904
NiBDP$_{Lit.}$ NMP/DMF	0.930
Average value	0.859
Standard deviation	0.045
Published values	

Galli *et al.* 2010 [11]	0.520
Hunag *et al.* 2020 [12]	0.856
Li *et al.* 2025 [13]	0.751
Wang *et al.* 2020 [14]	0.769
Calculated values	
Poreblazer [3]	0.712
Mercury [2]	0.852

Table S15. Determined pore volumes for **$[Zn(bdp)]_n$** from the nitrogen physisorption experiments. Different materials and washing procedures are compared to published and calculated values.

$[Zn(bdp)]_n$	
Material and washing procedure	**Pore Volume in cm^3/g**
$ZnBDP_B$ NMP/DMF	1.003
$ZnBDP_B$ DMSO/EtOH	1.052
$ZnBDP_B$ Soxhlet	0.951
$ZnBDP_{DBA}$ NMP/DMF	0.988
$ZnBDP_{Lit.}$ NMP/DMF	1.022
Average value	1.003
Standard deviation	0.038
Published values	
Galli *et al.* 2010 [11]	0.832
He *et al.* 2022 [15]	1.064
Cirujano *et al.* 2020 [16]	0.977
Xie *et al.* 2021 [17]	1.106
Calculated values	
Poreblazer [3]	0.916
Mercury [2]	1.010

Table S16. Determined pore volumes for **BUT-58** from the nitrogen physisorption experiments. Different materials and washing procedures are compared to published and calculated values.

BUT-58	
Material and washing procedure	**Pore Volume in cm^3/g**
$ZnBDP_{BA}$ NMP/DMF	0.428
$ZnBDP_{BA}$ DMSO/EtOH	0.453
$ZnBDP_{BA}$ Soxhlet	0.371
Average value	0.418
Standard deviation	0.042
Published values	
He *et al.* 2022 [15]	0.423
Calculated values	
Poreblazer [3]	0.427
Mercury [2]	0.503

IR Spectroscopy

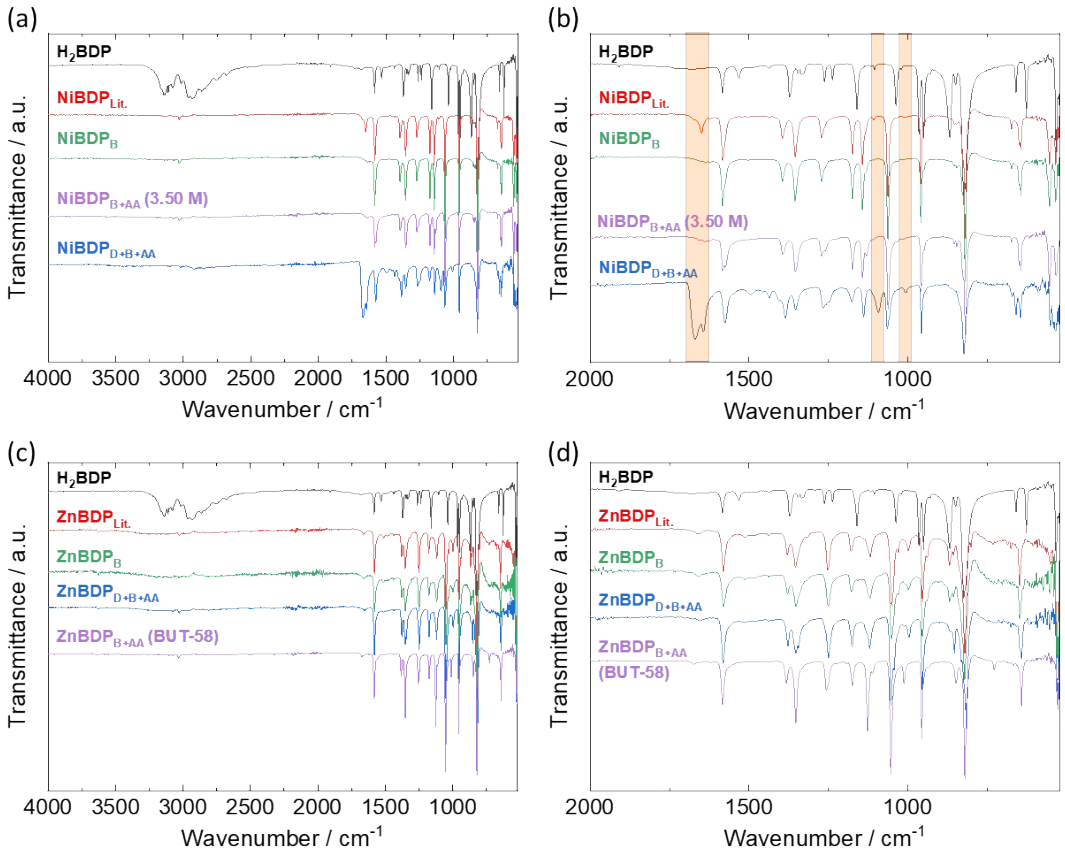

Figure S23. IR spectra of the respective samples after activation. (a) NiBDP full spectra, (b) Finger print region with highlighted DMF bands, (c) ZnBDP full spectra, (d) Finger print region. H_2bdp added for comparison to all sets.

The IR spectra of the MOFs are clearly dominated by the vibrational modes of the H_2bdp linker. However, no free linker can be observed in the samples, confirming a successful removal of linker residues during washing and activation. Despite the washing with NMP and DMF, only two samples: **NiBDP$_{Lit.}$** and **NiBDP$_{D+B+AA}$** show the presence of DMF bands (highlighted in orange in Figure S23b). These are also the two samples that were synthesized with DMF among the NiBDP samples. This observation suggests a certain amount of trapped DMF inside the structure, which is strongly bound to the framework.

Characterization of the filtrates remaining after MOF synthesis

To determine the composition of the solvent after the MOF syntheses, ^{1}H-NMR spectroscopy was conducted directly after cooling the reaction mixture. The MOF particles were previously removed by filtration. A small amount of CH_2Br_2 in DMSO-d6 was added as an internal standard to 500 µl of the filtrate. The observed organic species were identified.

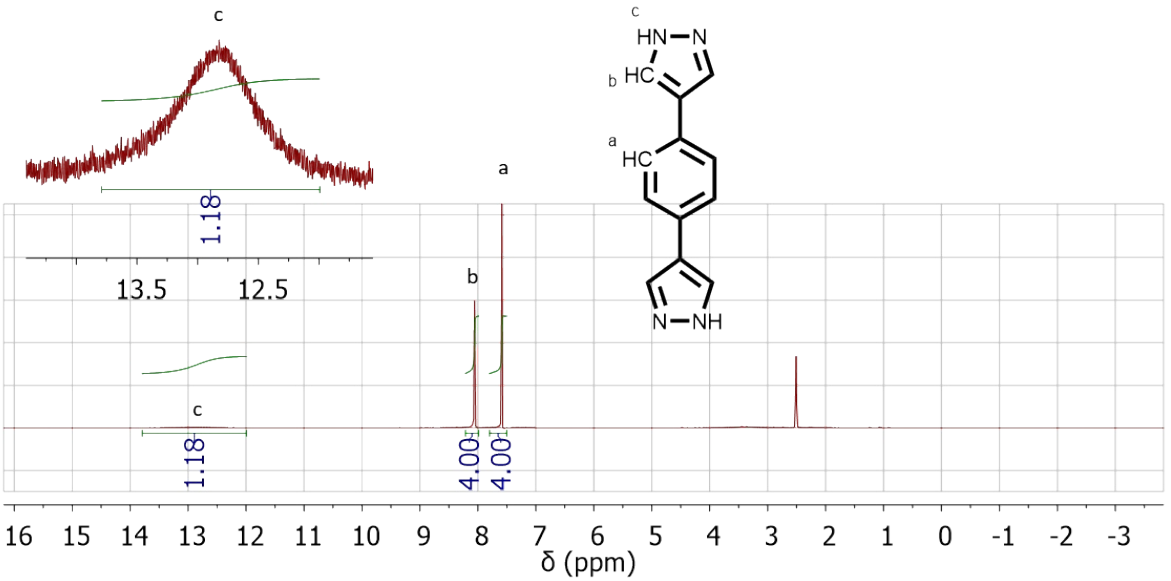

Figure S24. ^{1}H-NMR (300 MHz; DMSO-d6) of H_2bdp.

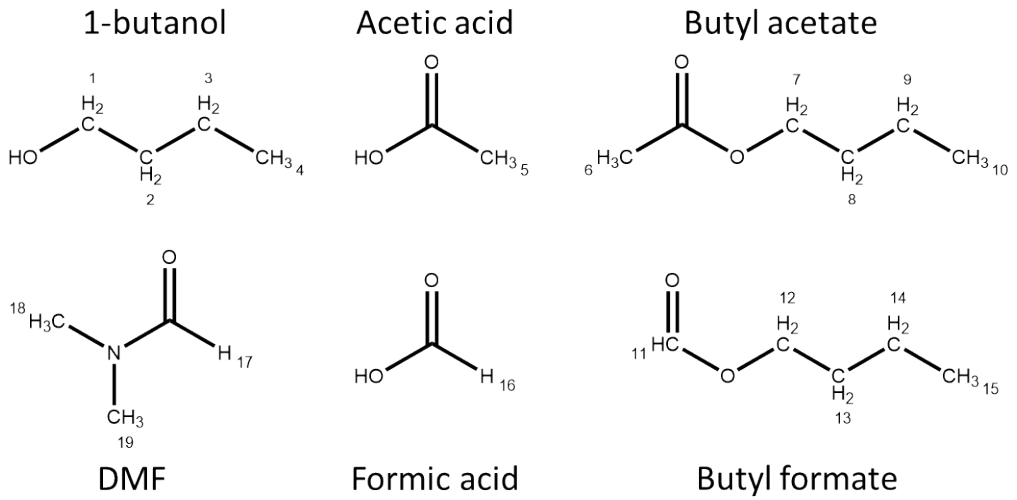

Figure S25. Observed organic species in the ^{1}H-NMR (300 MHz; DMSO-d6) of the MOF filtrate remaining after the synthesis. Protons are uniquely numbered.

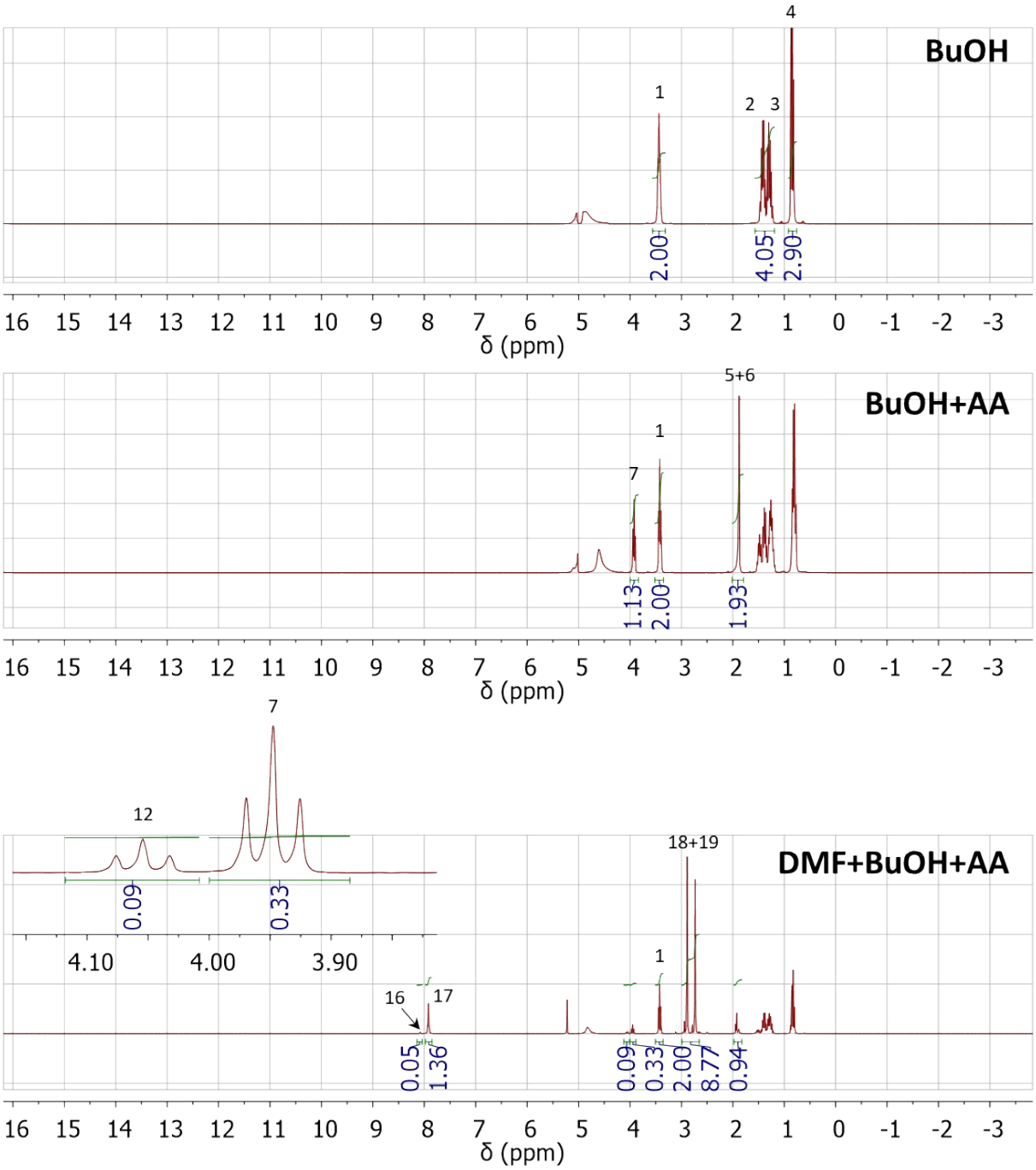

Figure S26. Full ^{1}H-NMR (300 MHz; DMSO-d6) spectra of the filtrate remaining after **NiBDP** synthesis: **NiBDP$_{B}$**, **NiBDP$_{B+AA}$**, **NiBDP$_{D+B+AA}$**. Spectra normalized to the primary butanol protons. Relevant signals attributed to protons of structures as shown in Figure S25.

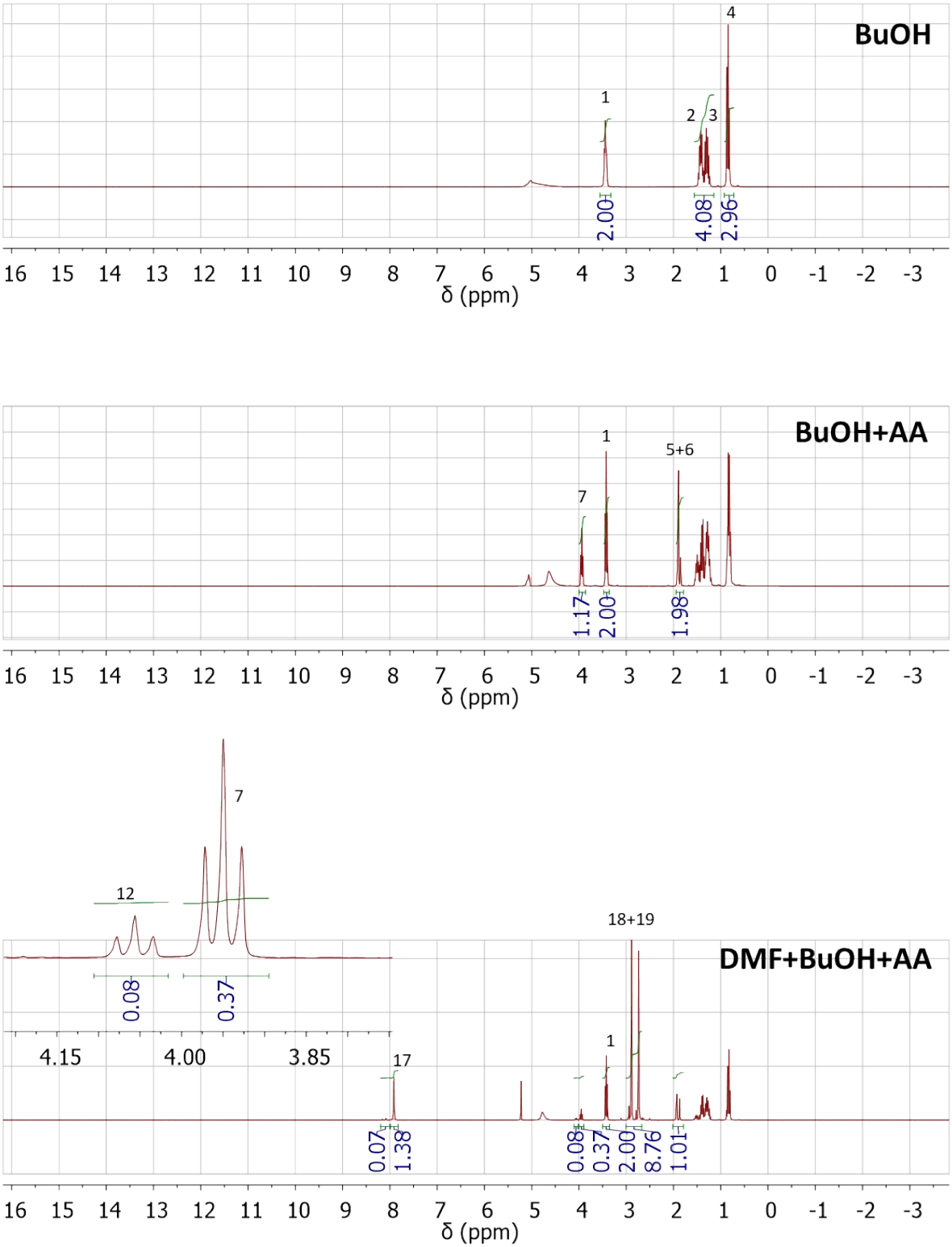

Figure S27. Full ^{1}H-NMR (300 MHz; DMSO-d6) spectra of the filtrate remaining after **ZnBDP** synthesis: **ZnBDP$_{B}$**, **ZnBDP$_{B+AA}$**, **ZnBDP$_{D+B+AA}$**. Spectra normalized to the primary butanol protons. Relevant signals attributed to protons of structures as shown in Figure S25.

The compositions of the filtrates remaining after NiBDP and ZnBDP syntheses are almost identical. The two different metals of the MOFs do not change the composition of the remaining solvent, which confirms equal catalytic activity of Zn^{2+} and Ni^{2+} for the esterification reactions. No residual H_2bdp could be detected in the solutions. In the syntheses performed in pure BuOH (**NiBDP$_B$** and **ZnBDP$_B$**) no changes to the butanol can be observed. For the binary DSS with butanol and acetic acid (**NiBDP$_{B+AA}$** and **ZnBDP$_{B+AA}$**), 36% and 37% of butanol have reacted to the butyl acetate, respectively, which is well in line with the predicted value of 35%. In the tertiary DSS mixture containing DMF, butanol, and acetic acid (**NiBDP$_{D+B+AA}$** and **ZnBDP$_{D+B+AA}$**), the observed reactions are more convoluted. Besides the butyl acetate already observed in the binary DSS, the tertiary mixture produces, in addition, butyl formate originating from the DMF decomposition products. A small amount of free formic acid can be detected (as a signal at δ = 8.08 ppm). A smaller fraction of butanol has reacted to the ester products, amounting to only 17 % and 18 % in the cases of **NiBDP$_{D+B+AA}$** and **ZnBDP$_{D+B+AA}$**, respectively. Considering only the butyl acetate, and then 14 % and 15 % of the butanol reacted to this specific product in the two respective cases. This fits adequately to the expected value of 13 % predicted by the kinetic model. The excess of reacted butanol can be explained by the shift of the chemical equilibrium due to the removal of water by the DMF during its decomposition. Thus, an excess of reacted butanol is expected.

The solid residue of the mother liquor was quantified after complete evaporation of the solvents. From each synthesis, 5 ml of the mother liquor was completely dried at 180°C over 24 h. The residual masses from the mentioned syntheses are summarized in Table S17.

The solid residue was resolvated in ultrapure HNO_3 (65 %) and diluted for ICP OES analysis to determine the metal content. The obtained values are recalculated for the amounts found in the initial MOF mother liquor and are summarized in Table S17. A can be seen the residual metal content in the solvent after MOF synthesis is on a scale of 0.1 % mass percent. Comparable to common catalyst contents during Fisher esterification reactions.

Table S17. Residual dry masses in the mother liquors after MOF synthesis in mg/L.

Synthesis	Residual mass (mg/L)	Residual metal content (mg/l)
NiBDP$_B$	142	16.27
NiBDP$_{B+AA}$	986	143.3
NiBDP$_{D+B+AA}$	436	29.77
ZnBDP$_B$	≈0*	4.37
ZnBDP$_{B+AA}$	574	89.39
ZnBDP$_{D+B+AA}$	538	86.11

*The mass difference was below the weighing error of the utilized scales.

MOF digestion

To verify the absence of solvent compounds in the final products, 7-10 mg of the MOFs were digested in 37 % DCl in D_2O, and then solubilized in DMSO-d6. Interestingly, at these pH conditions, both H_2bdp proton signals merge and appear as one singlet. Due to the magnetic interactions of the nickel, the width of the signals does not allow a deconvolution of the two peaks (Figure S28). In the ZnBDP digestions, the H_2bdp appears as an almost completely coinciding doublet (Figure S29). Only in the case of **NiBDP$_{D+B+AA}$**, the presence of DMF in the framework can be confirmed, which supports the results of the IR spectroscopy. In all other instances, the amounts of possible contaminants are below the detection levels.

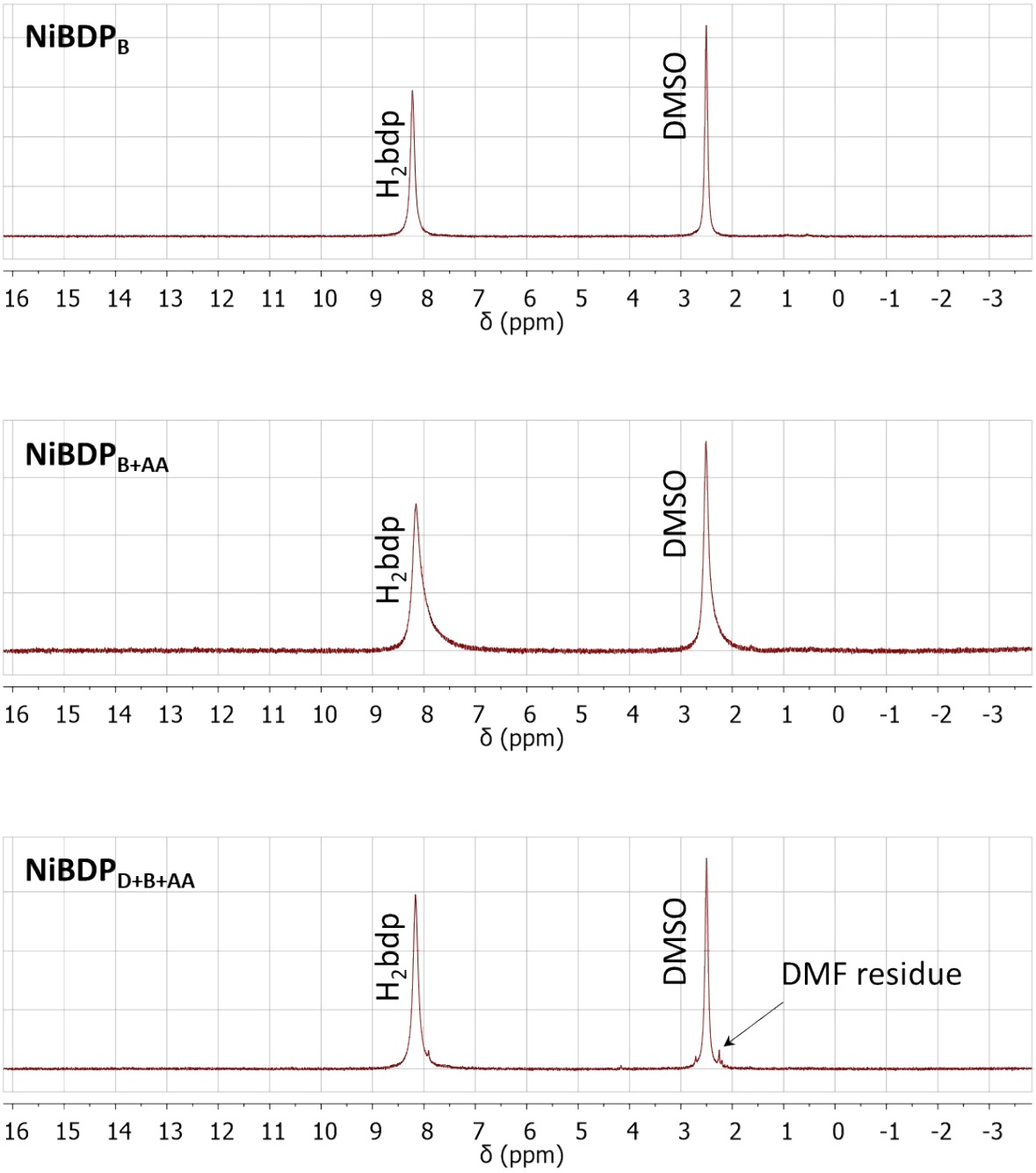

Figure S28. Full ^{1}H-NMR (300 MHz; DMSO-d6) spectra of the digested MOFs: **NiBDP$_B$**, **NiBDP$_{B+AA}$**, **NiBDP$_{D+B+AA}$**.

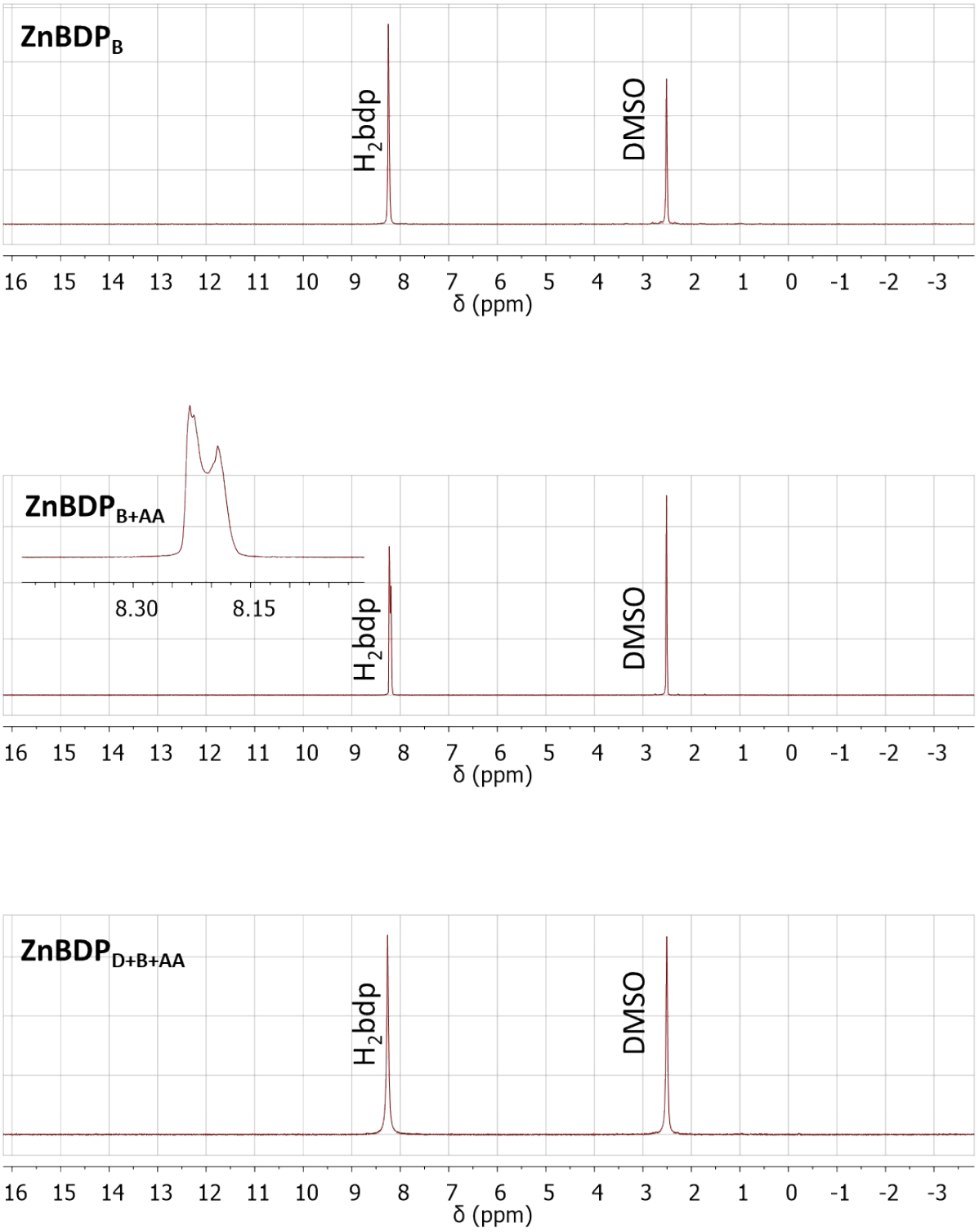

Figure S29. Full ^{1}H-NMR (300 MHz; DMSO-d6) spectra of the digested MOFs: **ZnBDP$_B$**, **ZnBDP$_{B+AA}$**, **ZnBDP$_{D+B+AA}$**.

References

1 V. Colombo, C. Montoro, A. Maspero, G. Palmisano, N. Masciocchi, S. Galli, E. Barea and J. A. Navarro, *J. Am. Chem. Soc.*, 2012, **134**, 12830–12843.

2 C. F. Macrae, I. Sovago, S. J. Cottrell, P. T. A. Galek, P. McCabe, E. Pidcock, M. Platings, G. P. Shields, J. S. Stevens, M. Towler and P. A. Wood, *J. Appl. Crystallogr.*, 2020, **53**, 226–235.

3 L. Sarkisov, R. Bueno-Perez, M. Sutharson and D. Fairen-Jimenez, *Chem. Mat.*, 2020, **32**, 9849–9867.

4 Accellrys, *Materials Studio 5.0*, San Diegeo, 2008.

5 U. Mueller, R. Förster, M. Hellmig, F. U. Huschmann, A. Kastner, P. Malecki, S. Pühringer, M. Röwer, K. Sparta, M. Steffien, M. Ühlein, P. Wilk and M. S. Weiss, *Eur. Phys. J. Plus*, 2015, **130**, 1–10.

6 T. G. G. Battye, L. Kontogiannis, O. Johnson, H. R. Powell and A. G. W. Leslie, *Acta crystallographica. Section D, Biological crystallography*, 2011, **67**, 271–281.

7 K. M. Sparta, M. Krug, U. Heinemann, U. Mueller and M. S. Weiss, *J. Appl. Crystallogr.*, 2016, **49**, 1085–1092.

8 G. M. Sheldrick, *Acta crystallographica. Section C, Structural chemistry*, 2015, **71**, 3–8.

9 Oxford Diffraction /Agilent Technologies UK Ltd, *CrysAlisPRO*, Yarnton, England.

10 Florent Boudoire, *chemical-kinetics*, GitHub, 2020.

11 S. Galli, N. Masciocchi, V. Colombo, A. Maspero, G. Palmisano, F. J. López-Garzón, M. Domingo-Garcia, I. Fernández-Morales, E. Barea and J. A. Navarro, *Chem. Mat.*, 2010, **22**, 1664–1672.

12 G. Huang, L. Yang, Q. Yin, Z.-B. Fang, X.-J. Hu, A.-A. Zhang, J. Jiang, T.-F. Liu and R. Cao, *Angew. Chem. Int. Ed. Engl.*, 2020, **59**, 4385–4390.

13 J. Li, N. Zhang, Q. Wang, B. Tian, Z. Li, J. Zhang, H. Xie, H. Gu and H. Zhao, *Chem. Eng. J.*, 2025, **515**, 163435.

14 Z. Wang, Q. Xie, Y. Wang, Y. Shu, C. Li and Y. Shen, *New J. Chem.*, 2020, **44**, 18319–18325.

15 T. He, X. J. Kong, Z. X. Bian, Y. Z. Zhang, G. R. Si, L. H. Xie, X. Q. Wu, H. Huang, Z. Chang, X. H. Bu, M. J. Zaworotko, Z. R. Nie and J. R. Li, *Nat. Mater.*, 2022, **21**, 689–695.

16 F. G. Cirujano, E. López-Maya, N. Almora-Barrios, A. Rubio-Gaspar, N. Martín, J. A. R. Navarro and C. Martí-Gastaldo, *Inorg. Chem.*, 2020, **59**, 18168–18173.

17 Q. Xie, W. Si, Y. Shen, Z. Wang and H. Uyama, *Nanoscale*, 2021, **13**, 16296–16306.